ELEMENTA Science of the Anthropocene

Ortega, I, et al. 2023. Anomalies of O_3, CO, C_2H_2, H_2CO, and C_2H_6 detected with multiple ground-based Fourier-transform infrared spectrometers and assessed with model simulation in 2020: COVID-19 lockdowns versus natural variability. *Elem Sci Anth*, 11: 1. DOI: https://doi.org/10.1525/elementa.2023.00015

RESEARCH ARTICLE

Anomalies of O_3, CO, C_2H_2, H_2CO, and C_2H_6 detected with multiple ground-based Fourier-transform infrared spectrometers and assessed with model simulation in 2020: COVID-19 lockdowns versus natural variability

Ivan Ortega[1,*], Benjamin Gaubert[1], James W. Hannigan[1], Guy Brasseur[1,2], Helen M. Worden[1], Thomas Blumenstock[3], Hao Fu[4], Frank Hase[3], Pascal Jeseck[4], Nicholas Jones[5], Cheng Liu[6], Emmanuel Mahieu[7], Isamu Morino[8], Isao Murata[9], Justus Notholt[10], Mathias Palm[10], Amelie Röhling[3], Yao Té[4], Kimberly Strong[11], Youwen Sun[12], and Shoma Yamanouchi[11]

Anomalies of tropospheric columns of ozone (O_3), carbon monoxide (CO), acetylene (C_2H_2), formaldehyde (H_2CO), and ethane (C_2H_6) are quantified during the 2020 stringent COVID-19 world-wide lockdown using multiple ground-based Fourier-transform infrared spectrometers covering urban and remote conditions. We applied an exponential smoothing forecasting approach to the data sets to estimate business-as-usual values for 2020, which are then contrasted with actual observations. The Community Atmosphere Model with chemistry (CAM-chem) is used to simulate the same gases using lockdown-adjusted and business-as-usual emissions. The role of meteorology, or natural variability, is assessed with additional CAM-chem simulations. The tropospheric column of O_3 declined between March and May 2020 for most sites with a mean decrease of 9.2% $\pm$ 4.7%. Simulations reproduce these anomalies, especially under background conditions where natural variability explains up to 80% of the decline for sites in the Northern Hemisphere. While urban sites show a reduction between 1% and 12% in tropospheric CO, the remote sites do not show a significant change. Overall, CAM-chem simulations capture the magnitude of the anomalies and in many cases natural variability and lockdowns have opposite effects. We further used the long-term record of the Measurements of Pollution in the Troposphere (MOPITT) satellite instrument to capture global anomalies of CO. Reductions of CO vary highly across regions but North America and Europe registered lower values in March 2020. The absence of CO reduction in April and May, concomitant with reductions of anthropogenic emissions, is explained by a negative anomaly in the hydroxyl radical (OH) found with CAM-chem. The implications of these findings are discussed for methane (CH_4), which shows a positive lifetime anomaly during the COVID-19 lockdown period. The fossil fuel combustion by-product tracer C_2H_2 shows a mean drop of 13.6% $\pm$ 8.3% in urban Northern Hemisphere sites due to the reduction in emissions and in some sites exacerbated by natural variability. For some sites with anthropogenic influence there is a decrease in C_2H_6. The simulations capture the anomalies but the main cause may be related to natural variability. H_2CO declined during the stringent 2020 lockdown in all urban sites explained by reductions in emissions of precursors.

Keywords: COVID-19, FTIR, CAM-chem, Natural variability

[1] Atmospheric Chemistry Observations & Modeling, National Center for Atmospheric Research, Boulder, CO, USA

[2] Environmental Modeling Group, Max Planck Institute for Meteorology, Hamburg, Germany

[3] Karlsruhe Institute of Technology, Institute of Meteorology and Climate Research (IMK-ASF), Karlsruhe, Germany

[4] Laboratoire d'Etudes du Rayonnement et de la Matière en Astrophysique et Atmosphères, Sorbonne Université, CNRS, Observatoire de Paris, PSL Université, Paris, France

[5] School of Physics, University of Wollongong, Wollongong, Australia

[6] Department of Precision Machinery and Precision Instrumentation, University of Science and Technology of China, Hefei, China

[7] Institute of Astrophysics and Geophysics, UR SPHERES, University of Liège, Liège, Belgium

[8] National Institute for Environmental Studies, Tsukuba, Japan

[9] Graduate School of Environmental Studies, Tohoku University, Sendai, Japan

[10] Institute of Environmental Physics, University of Bremen, Germany

[11] Department of Physics, University of Toronto, Toronto, Ontario, Canada

[12] Key Laboratory of Environmental Optics and Technology, Anhui Institute of Optics and Fine Mechanics, HFIPS, Chinese Academy of Sciences, Hefei, China

* Corresponding author:
Email: iortega@ucar.edu

1. Introduction

The stringent 2020 worldwide lockdown due to the COVID-19 pandemic provided an opportunity to study the impact of reduced anthropogenic activity on atmospheric composition. Surface in-situ and satellite platforms have been predominantly used in the analysis of stay-at-home impacts on air quality. A comprehensive overview of multiple studies related to COVID-19 lockdown impacts on air quality have been documented in Gkatzelis et al. (2021) and data have been digitized and are available on a dedicated website (https://covid-aqs.fz-juelich.de/). Gkatzelis et al. (2021) pointed out that nitrogen dioxide (NO_2), $PM_{2.5}$, and ozone (O_3) have been broadly studied while other compounds are found to be understudied. Another review by Addas and Maghrabi (2021) found that the majority of studies focused over Asia and that more than 60% of the studies included NO_2. A list of publications on emissions and atmospheric compositions is available online from the Analysis of eMIssions usinG Observations working group of International Global Atmospheric Chemistry (https://amigo.aeronomie.be/index.php/covid-19-publications/peer-reviewed).

O_3 varies nonlinearly with changes in emissions and meteorology (Kroll et al., 2020) and therefore both positive and negative anomalies were found due to photochemical regime change and meteorological anomalies around the world (Ordóñez et al., 2020; Deroubaix et al., 2021; Gaubert et al., 2021; Grange et al., 2021; Liu et al., 2021; Zhang et al., 2022). Steinbrecht et al. (2021) reported a widespread decline of 7% in O_3 in the free troposphere in the Northern extratropics from multiple observations. Bouarar et al. (2021) assessed the cause of the reduction in O_3 using global model simulations in the free troposphere and concluded that one third in the decrease was attributable to reduction of surface emissions, primarily due to a global reduction of NO_x emissions of at least 15% (Levelt et al., 2021; Miyazaki et al., 2021), another one third attributed to reduction in air traffic and the remaining to meteorological conditions in the extra tropics of the Northern Hemisphere.

Analysis of other gases, in particular, carbon monoxide (CO) and volatile organic compounds (VOC) is limited to a few studies (Levelt et al., 2021; Stavrakou et al., 2021). A global analysis reported in Sokhi et al. (2021) shows lower CO concentrations relative to a few years in the past within major cities, although the study points out the importance of other complex factors such as dispersion, temperature, and precipitation. Zhou et al. (2021) used surface and TROPOMI and IASI satellites observations to quantify the change of CO in China observing a decrease in the surface between 8% and 27%, while satellites detected a decrease of 2%–11%, however an increase of CO columns of 8.8% was also observed in South China attributed to fire emissions transported from Southeast Asia. Sun et al. (2021) examined changes in formaldehyde (H_2CO) during the early stage of the COVID-19 pandemic (January to April 2020) and found a decrease in Northern China while some increase in other parts of the world was likely linked to open fire emissions, although linking changes to COVID-19 in most regions is difficult to assess due to the natural variability of H_2CO (Levelt et al., 2021).

For the first time, we examine changes of several tropospheric gases during the stringent 2020 world-wide lockdown detected with ground-based Fourier-transform infrared spectrometers (FTIR) at multiple sites, most of them within the Network for Detection of Atmospheric Composition Change (NDACC, www.ndacc.org). These changes are assessed with model simulations in order to understand the possible impact of COVID-19 lockdown emissions and the role of natural variability, primarily the record-low stratospheric O_3 depletion in the Arctic in 2020 (Manney et al., 2020). It has been shown elsewhere that the growth rate of methane (CH_4) was not slowed by the COVID-19 induced changes in the emissions (e.g., Laughner et al., 2021). It is essential to quantify the role of potential interannual variability in hydroxyl radical (OH) on the CH_4 growth rate in order to accurately quantify CH_4 emission (Zhao et al., 2020). Global chemistry models estimate a significant reduction in OH driven by NO_x emissions reduction, but with a significant role of natural variability (Gaubert et al., 2021; Laughner et al., 2021; Miyazaki et al., 2021). Recently, Stevenson et al. (2022) argued that nearly half of the CH_4 growth rate in 2020 could have been a result of the emissions reduction of nitrogen oxides (NO_x), CO, and nonmethane volatile organic compounds (NMVOCs). Qu et al. (2022) estimated that only 14% of the growth rate increase was due to the decrease in tropospheric OH. McNorton et al. (2022) showed that the growth rate was driven by a continued increasing trend in CH_4 emissions but only considered a climatological OH sink. In this work, we further used model simulations to estimate anomalies in lifetimes of CH_4 and CO during the 2020 stringent COVID-19 period.

Ground-based long-term monitoring of upper tropospheric and lower stratosphere (UTLS) composition during the 2020 stringent period is limited. Most studies on atmospheric composition changes during the COVID-19 pandemic have focused on surface observations, with only a few employing numerical simulations and aircraft observations to report changes above the boundary layer (Clark et al., 2021; Cristofanelli et al., 2021; Nussbaumer et al., 2022; Reifenberg et al., 2022). To bridge this gap, we have analyzed FTIR data and focused on O_3 and CO anomalies in the UTLS, as these gases have high sensitivity in these layers.

2. Methods and data

2.1. Ground-based NDACC FTIR observations

The data presented here are collected with globally dispersed ground-based FTIR stations. **Figure 1** shows the locations of the sites that contributed data to this study. **Table 1** contains more details for each site ordered by latitude and lists the species that were available at each site. Most of the stations are part of the NDACC. Currently, the stations at Paris, Karlsruhe, and Hefei are not officially part of NDACC though their observation strategy is similar to the InfraRed Working Group (IRWG) standards (www2.acom.ucar.edu/irwg). The sites are located in either urban (or semi-urban) or remote locations and the initial year of

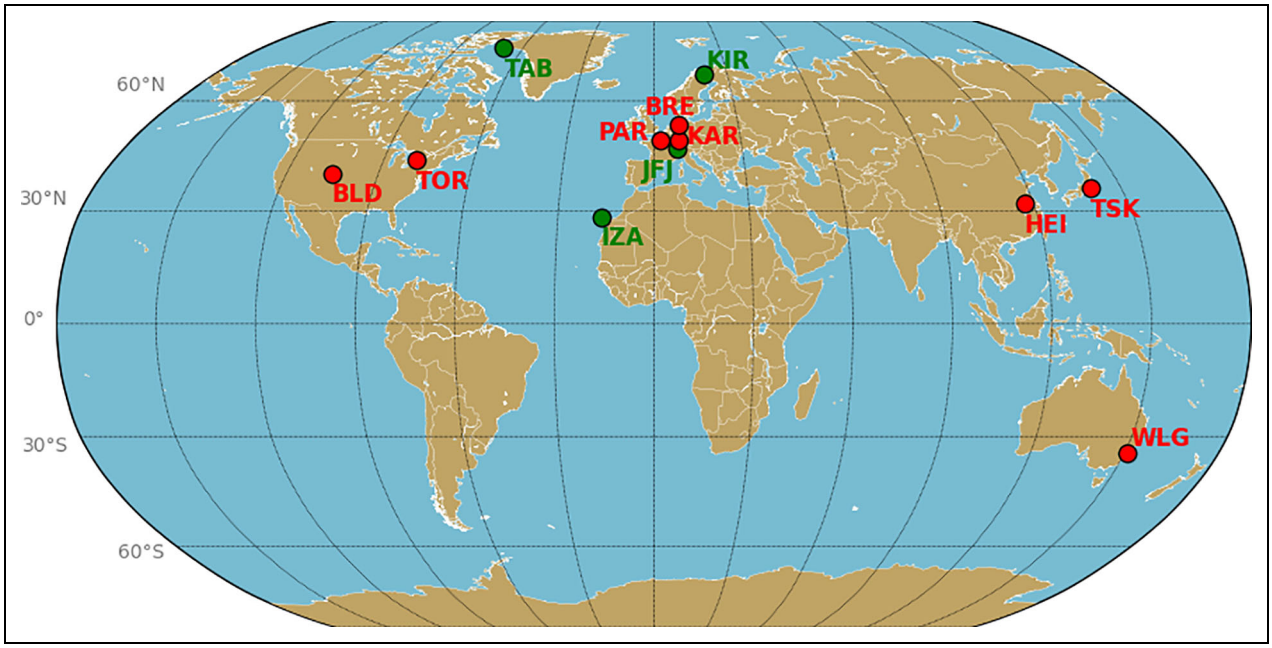

Figure 1. Location of FTIR stations contributing to this study. Red and green sites are considered urban and remote sites, respectively.

Table 1. List of stations with location details contributing to this study

Station	N. Latitude [°]	E. Longitude [°]	Altitude [m.a.s.l]	Type	Species
Thule (TAB)	76.53	291.26	225	Remote	O_3, CO, H_2CO, C_2H_6, C_2H_2
Kiruna (KIR)	67.84	20.41	420	Remote	O_3, CO, H_2CO, C_2H_6
Bremen (BRE)	53.10	8.90	27	Urban	O_3, CO, H_2CO, C_2H_6
Karlsruhe (KAR)	49.10	8.42	60	Urban	CO, H_2CO, C_2H_6
Paris (PAR)	48.85	2.36	60	Urban	CO, H_2CO, C_2H_6
Jungfraujoch (JFJ)	46.55	7.98	3,580	Remote	O_3, CO, H_2CO, C_2H_6, C_2H_2
Toronto (TOR)	43.66	280.60	174	Urban	O_3, CO, H_2CO, C_2H_6, C_2H_2
Boulder (BLD)	40.04	254.76	1,612	Urban	O_3, CO, H_2CO, C_2H_6, C_2H_2
Tsukuba (TSK)	36.05	140.12	31	Urban	O_3, CO, H_2CO, C_2H_6, C_2H_2
Hefei (HEI)	31.91	117.17	34	Urban	O_3, CO, H_2CO, C_2H_6
Izaña (IZA)	28.30	343.52	2,370	Remote	O_3, CO, H_2CO, C_2H_6
Wollongong (WLG)	−34.41	150.88	30	Urban	O_3, CO, H_2CO, C_2H_2

operation varies by site but the period between 2010 and 2020 is covered by all sites and used in the long-term analysis for consistency, except Hefei that started observations in 2015. These sites continued observations during lockdowns in 2020. Unfortunately, several other NDACC/IRWG stations could not perform or had limited measurements during the period of interest in this study (March–May 2020).

The FTIR instruments acquire direct sun spectra in selected spectral band regions (to maximize signal to noise) through the mid-infrared with high-resolution, typically with an optical path difference of 250 cm (but minimal of 180 cm) resulting in nominal spectral resolution of about 0.004 cm^{-1} using liquid nitrogen-cooled InSb (approximately 1,850–10,000 cm^{-1}) and HgCdTe (approximately 600–6,000 cm^{-1}) detectors. Measurements are performed routinely under cloud free conditions.

The operational retrieval strategies for O_3, CO, C_2H_6, and H_2CO have been consistently applied by all sites per the guidelines of the IRWG (www2.acom.ucar.edu/irwg) including a common vertical grid above 7 km and adjusted grid below to accommodate the local station altitude. C_2H_2 is not a "standard" retrieved gas in the IRWG, however, it has been successfully retrieved in several other studies (Vigouroux et al., 2012; Viatte et al., 2014; Ortega et al., 2021). Briefly, all the gases are retrieved using either the retrieval code PROFITT9.6 (Kiruna, Karlsruhe, Hefei, Izaña, and Paris) or SFIT4 (Thule,

Bremen, Jungfraujoch, Toronto, Boulder, Tsukuba, and Wollongong). A description of both retrieval algorithms is found in Hase et al. (2004) illustrating the agreement in retrieved data products and sensitivity. A thorough description of the retrieval inversion is given in more detail elsewhere (e.g., Rodgers, 2000).

All the gases have good vertical sensitivity throughout the troposphere with C_2H_2, C_2H_6, and H_2CO showing at least one degrees of freedom for signal (DOFS) while O_3 and CO contain 4–5 and 2–3 DOFS, respectively. The total error budget is obtained by an error propagation of the random and systematic uncertainty obtained in the retrieval. **Table 2** includes a summary of the uncertainty, DOFS, and references for further details. The data used here are stored as standard IRWG files at the NDACC Data Handling Facility for all NDACC stations.

Tropospheric weighted volume mixing ratios (wVMR) are used to estimate anomalies. wVMR are calculated with the expression below:

$$\mathrm{wVMR} = \frac{\sum_{z=1}^{n} x_z \cdot K_z}{\sum_{z=1}^{n} K_z} \quad (1)$$

where z is the altitude layer on the retrieval grid, x_z is the retrieved mixing ratio profile in that layer, and k_z is the associated air mass. The influence of the tropopause is excluded by using a maximum altitude that is lower than the tropopause height. We use the latitudinal dependent annual cycle tropopause height from the National Centers for Environmental Prediction (Kalnay et al., 1996) and calculate the maximum height as the tropopause height minus the standard deviation obtained in the annual cycle. A similar approach has been recently applied in Hannigan et al. (2022) to determine tropospheric columns of carbonyl sulfide within the NDACC/IRWG. Anomalies in the UTLS are also calculated for O_3 and CO. For consistency among all sites we use the tropopause ± 4 km, which typically contains the second DOF.

Table 2. Summary of degrees of freedom for signal (DOFS) and random and systematic uncertainties for each gas

Gas	DOFS	Random [%]	Systematic [%]	Reference
O_3	4–5	~3	~9	Vigouroux et al. (2015)
CO	2–3	~1	~3	Sha et al. (2021)
H_2CO	1	~8	~13	Vigouroux et al. (2018)
C_2H_6	1.5	~2.5	~6	Franco et al. (2015)
C_2H_2	1.5	~12	~6	Viatte et al. (2014)

2.2. CAM-chem simulations

The Community Atmosphere Model with chemistry (CAM-chem) within the Community Earth System Model (CESM) framework version 2.2 described in detail in Danabasoglu et al. (2020) is used for the simulations. A thorough description of the model simulations during COVID-19 lockdowns is given by Gaubert et al. (2021) and Bouarar et al. (2021). **Table 3** shows a summary of the different model parameters used in the simulations. A main difference consists of an update to the anthropogenic emissions (CAMS_GLOB_ANT v5.1). To account for the effect of the COVID-19 lockdowns, we follow the emission reductions estimated in the Daily CONFORM v2.1 (COvid-19 adjustmeNt Factors fOR eMissions) (Doumbia et al., 2021).

Bouarar et al. (2021) describes in detail several model simulations to obtain a quantitative response of different parameters considered such as the reduction in air traffic, surface emission reductions, and meteorological conditions, including the effect of the significant springtime ozone depletion in the Arctic in 2020. In this work, we do not aim to quantitatively analyze the effect of all parameters. Rather, we focus on assessing the impact of the stay-at-home response in comparison to a business-as-usual scenario, while also quantifying the effect of natural variability. Natural variability, in this context, pertains to meteorological variations that occur in the absence of any changes in emissions from anthropogenic and biomass burning sources. For the natural variability simulation, we utilized repeated anthropogenic and fire emissions from the year 2020, in conjunction with greenhouse gas levels from the same year. Our simulation commenced on January 1, 2001. Therefore the anomalies obtained from this simulation only account for changes in natural variability such as meteorology and related feedback on atmospheric composition (e.g., biogenic emissions responses to temperature). Note that the calculated anomalies use the same time period as the FTIR observations, which spanned from 2010 to 2020. In all cases, the simulations are nudged to MERRA-2 temperatures and winds at every physical step (30 mins). Furthermore, in order to evaluate changes of the downward transport of stratospheric O_3 into the troposphere due to the exceptional ozone depletion in the Arctic, we use a stratospheric tagged ozone in the simulations (Emmons et al., 2012). **Table 4** provides an overview of the main model simulation cases utilized in this study. The information presented in the table includes the name of each simulation case, a brief description of the model setup, and specific details used. Simulations were extracted for each site and to account for limited vertical profile sensitivity of the FTIR, the simulated profiles were smoothed by the mean FTIR averaging kernels at each site (Rodgers and Connor, 2003). For consistency with the FTIR, tropospheric wVMR are also used here. Our goal is to evaluate the relative differences observed during the stringent worldwide COVID-19 lockdown, rather than validate the magnitude of the simulations. Previous studies by Gaubert et al. (2021)

Table 3. Summary of the CAM-chem model parameters

Model Component	Model Input	Reference
Chemistry of gases and aerosols	Model for O_3 and Related chemical Tracers (MOZART) chemistry mechanisms in tde Troposphere Stratosphere (TS1)	Emmons et al. (2020)
Aerosol concentrations and size distribution	Derived from the 4-mode Modal Aerosol Model (MAM4)	Liu et al. (2016); Mills et al. (2016)
Meteorological conditions	Nudged using the MERRA-2 analysis	Gelaro et al. (2017)
Biogenic emissions	From the Model of Emissions of Gases and Aerosols from Nature	Guenther et al. (2012)
Biomass burning emissions	Daily Quick-Fire Emissions Dataset	Darmenov and da Silva (2014)
Anthropogenic surface emissions	Copernicus Atmosphere Monitoring Service (CAMS) global inventory	Soulie et al. (2023)

CAM-chem = Community Atmosphere Model with chemistry.

Table 4. Overview of the model simulations used in the analysis

Simulation Name	Description	Details
Clim	Baseline case for climatology (2010–2019)	Daily emissions with meteorology
Control	Baseline case for 2020	2020 daily emissions with no COVID-19 effects and with 2020 meteorology
COVID-19	Effects of combined adjustments in 2020 surface and aircraft emissions	Same as Control, but with surface and aircraft emissions adjusted for COVID-19 lockdown effects
$Clim_{NAT}$	Effects of natural variability	Same as Control but with 2020 emissions repeated in past years

and Bouarar et al. (2021) have demonstrated the ability of CAM-chem to accurately reproduce O_3 anomalies during COVID-19 impacts. Ortega et al. (2021) conducted a comparison of long-term CAM-chem simulations of tropospheric species with FTIR at Boulder, Colorado, and found that the model generally represents seasonal variations of all gases well, though it often underestimates magnitudes. Similarly, Gaubert et al. (2020) compared CAM-chem simulations using aircraft measurements taken in Korea and found a negative bias for CO but a good agreement for O_3. Recently, Albores et al. (2023) compared CAM-chem simulations against satellite and ground-based column CO observations over North America and showed that the model generally underestimated CO from fires but adequately reproduced spatial and temporal variability. Since the model accurately reproduces the seasonal variation of all gases, we can use it with confidence to observe relative differences during the COVID-19 lockdown.

2.3. Extracting the 2020 signal from the NDACC time series

A baseline (or reference) period is needed in order to calculate anomalies for each chemical species during 2020. Using a similar period as in 2020 but from past years, for example, 2019, or even climatological values that then are compared to 2020 is a common approach. However, uncertainties may be present due to different synoptic meteorological conditions. Furthermore, taking into account decreasing (or increasing) trends is important when constructing a reference period in order to avoid significant biases in the results. For example, Northern Hemispheric CO has been decreasing significantly in the past 2 decades (Worden et al., 2013; Buchholz et al., 2021), and using climatology mean values as the baseline for the comparison during stringent months in 2020 would yield large errors due to the weighted values in earlier years. CO can also present large interannual variability, for example, rising emissions from wildfires in August in North America (Buchholz et al., 2022), and a simple extrapolation may result in additional errors. In this study, we applied an innovative methodology to predict monthly business-as-usual values for the FTIR observations in 2019 and 2020, leveraging the monthly time series data from 2010 to 2018. This method is only applied to observations. For the simulations, the business-as-usual scenario is defined by the Control 2020.

The predicted data are produced using a probabilistic exponential smoothing method taking into account trends (Holt, 2004). Exponential smoothing methods are weighted averages of the past observations, with the weights decaying exponentially as the observations get older, that is, the more recent the observation, the higher the associated weight. We utilize DARTS, which is an open source Python library for manipulation and forecasting of time series (Herzen et al., 2022; https://unit8co.github.io/darts/).

The evaluation of the exponential smoothing model consists of 2 different parts. First, the model is evaluated using the fitting residuals of the model in the period used to construct the prediction, that is, 2010–2018. The residuals, difference between the fitted model and actual

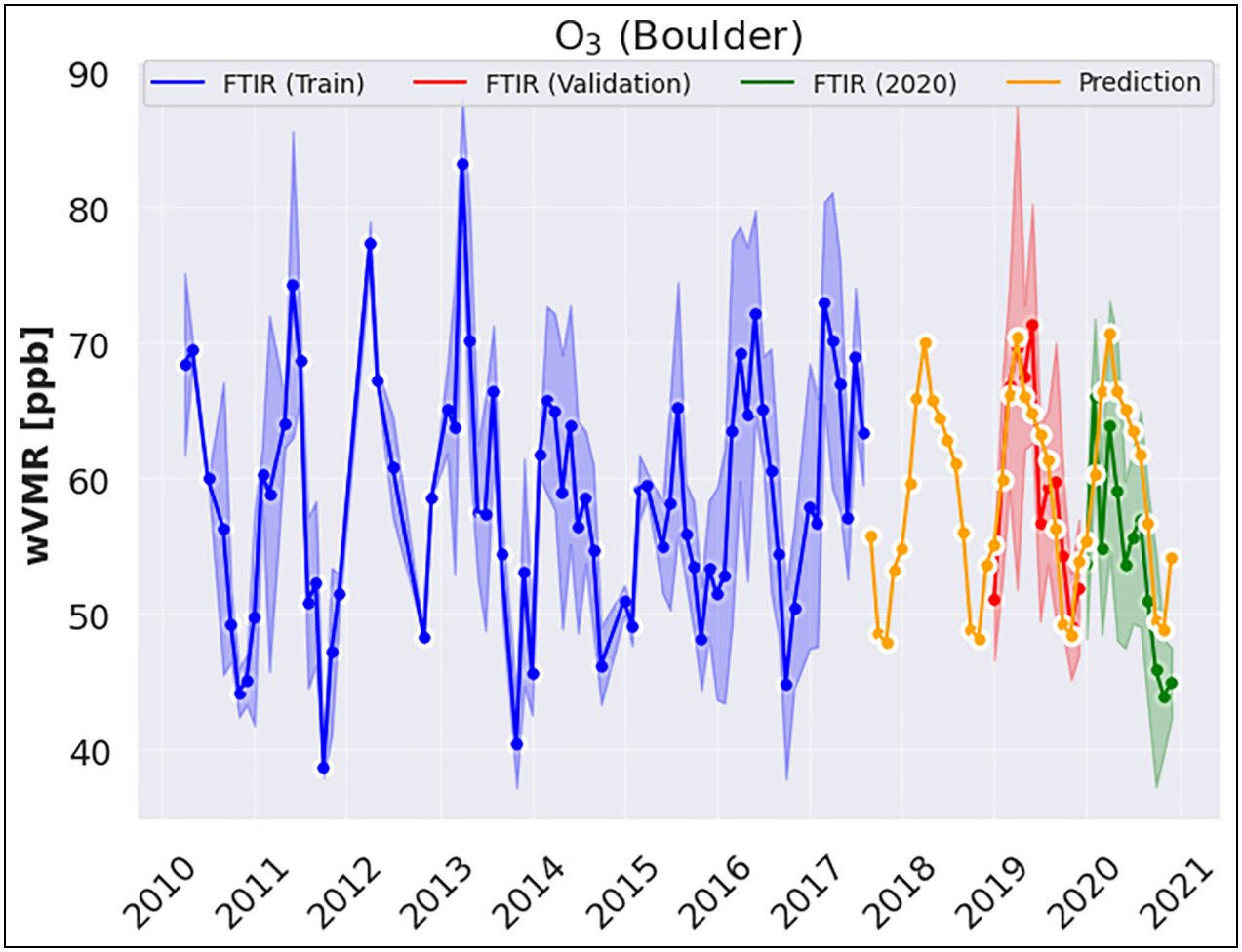

Figure 2. Time series of monthly mean O_3 weighted volume mixing ratios (wVMR) at Boulder, Colorado. The blue line represents the observations used to train the model and predict 2018–2020 monthly values (orange), which then are assessed in 2019 during the validation period (red) and calculate anomalies during the COVID-19 stringent period in 2020 using actual observations (green). The shaded area represent the standard deviation.

observations, are captured and some statistics are evaluated. For example, residuals with a mean close to zero and uncorrelated residuals are ideal. Second, the accuracy of the prediction is determined by comparing with actual observations not used when fitting the model prediction, in this case in 2019. **Figure 2** shows an example of the reference period construction using monthly mean time series of O_3 at the Boulder, Colorado, station. A major instrument upgrade occurred in most of 2018, hence the 2010–2017 period (blue) is used to train the model and predict 2018–2020 (orange). The red period shows the data used for the validation in 2019 and the green period represents the observations in 2020 to calculate anomalies. The validation period in 2018–2019 consists of the quantitative comparison of the prediction and actual observations during coincident months. A bias is estimated using the mean absolute percent error (MAPE) calculated with the following equation:

$$\mathrm{MAPE} = \frac{1}{n}\sum_{t=1}^{n}\frac{A_t - P_t}{A_t} \qquad (2)$$

where n is the number of coincident months in 2019, A_t is the actual FTIR wVMR, and P_t is the predicted wVMR. The MAPE value calculated for the example given in **Figure 2** is −0.41%. An advantage of calculating the bias is that the model predicted values are further corrected to estimate business-as-usual values in 2020. In the following sections, results are shown only for sites when the forecasting approach is applied successfully, MAPE values are low, typically lower than 20%, and the number of days for each month in 2020 are checked individually. For example, due to local restrictions Paris stopped observations in mid March and resumed observations early in May 2020. Observations at Bremen were also limited to March and April only.

3. Results

3.1. Anomalies of O_3 in the troposphere

Figure 3 shows O_3 results for Boulder, Colorado. The monthly mean wVMR values are shown on top for the FTIR (left) and CAM-chem simulations (right). The FTIR observations and predicted (business-as-usual) wVMR in 2020 are shown in red and orange, respectively. To quantify anomalies, the relative difference is calculated as the fraction of the difference between actual observations and the predicted 2020 divided by the predicted value itself.

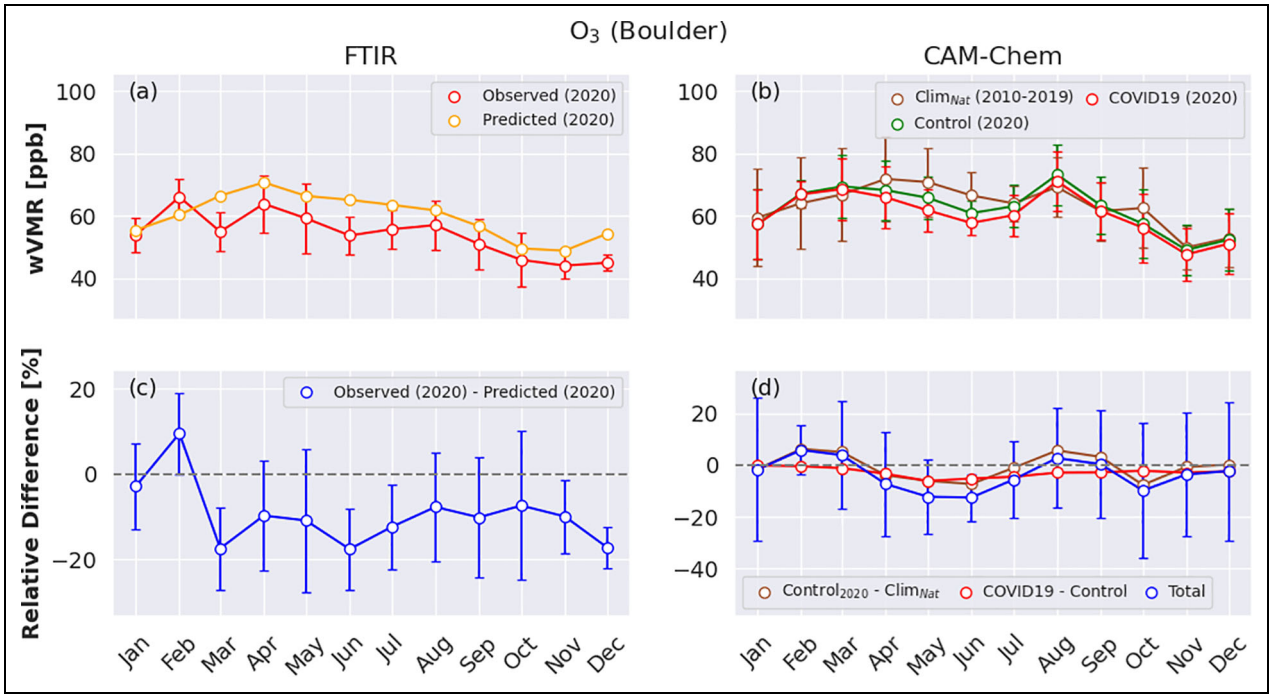

Figure 3. (a) Monthly mean weighted volume mixing ratios (wVMR) of O_3 observed (red) and predicted business-as-usual in 2020 (orange) at Boulder, Colorado. (b) CAM-chem simulations for the control scenario in 2020 (green), COVID-19 adjusted emission scenario (red), and natural variability climatology simulations (brown). (c) Illustrates the relative differences between the observations and predicted levels for each month in 2020. (d) Relative differences between the COVID-19 and control (red) and between the control and natural variability simulations (brown), with the combined effect of COVID-19 lockdown and natural variability depicted in blue. A comprehensive overview of the various simulations and methods used to obtain them is available in **Table 4**.

This is illustrated in the bottom plots. For CAM-chem, the monthly mean natural variability ($Clim_{NAT}$) using the 2010–2019 period, Control (2020), and adjusted COVID-19 (2020) simulations are shown in brown, green, and red, respectively (see **Table 4** for additional details). To quantify the impact of the stringent COVID-19 lockdowns on the simulations, the difference between COVID-19 and Control (2020) (i.e., business-as-usual) simulations has been considered (see the legend for COVID19–Control). The difference between Control and natural variability highlights the effect of the natural variability (see $Control_{2020}$–$Clim_{NAT}$). Finally, the total anomaly in the simulations is derived by summing the anomalies from both effects COVID-19 lockdowns and natural variability (blue). The error bars in **Figure 3(a)** and **(b)** represent the standard deviations, while error bars in **Figure 3(c)** and **(d)** represent the uncertainty propagated from the standard deviations within each month.

The FTIR O_3 anomalies at Boulder reveal that after March 2020, the ozone decreased by about 10% with lower levels between March–June, which coincides with the stringent lockdowns in the region, across the United States, and in many parts of the world. Interestingly, ozone remained low for the rest of 2020. The total anomalies in the simulations are consistent with observations with larger positive values in February followed by a sharp decrease in March through July. Note that between April and June 2020 both the natural variability and COVID-19 lockdowns played an equal role in the decrease of O_3 and after July 2020 the natural variability is positive due to fires in 2020 while COVID-19 restrictions show still a decrease. This is likely the reason for the negative anomalies in the observations, that is, without the effect of COVID-19 restriction, the magnitude of the O_3 anomalies within the fire plumes would be positive.

The above methodology is applied to all sites and **Figure 4** shows a map with anomalies calculated between March and May 2020 for all sites. This period corresponds to stringent COVID-19 lockdowns across the Northern Hemisphere, primarily North America and Europe according to COVID-19 Google mobility trends (see https://ourworldindata.org/covid-mobility-trends). The orange bars are FTIR anomalies; the CAM-chem blue bars are the total anomalies estimated from the COVID-19 (red) and natural variability (brown) contributions. All sites show a decline of O_3 in the troposphere with a global mean of $9.2\% \pm 4.7\%$ during March–May 2020, in agreement with Steinbrecht et al. (2021) and Ziemke et al. (2022). The total decrease is well captured in the CAM-chem simulations, especially for the remote sites, for example, Thule, Kiruna, Jungfraujoch, where natural variability plays a more important role in the decrease in O_3, explaining up to 80% of the decrease. In urban sites, the total decrease is not totally captured, likely COVID-19 emission precursors are underestimated on these sites, and natural variability explains about a third of the decrease.

Table 5 provides a detailed summary of the mean changes in tropospheric O_3, comparing the observations

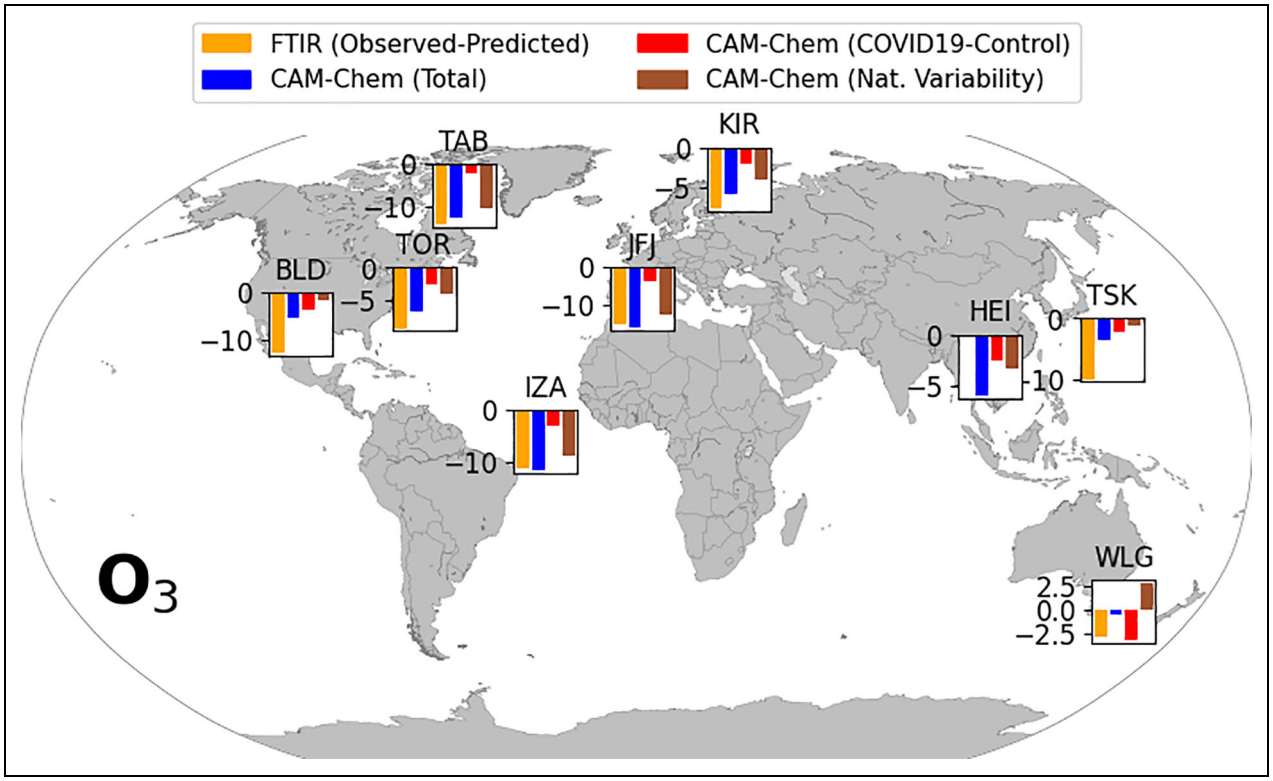

Figure 4. Map with tropospheric anomalies of O_3 at different sites, expressed as a percentage and estimated using mean values obtained between March and May 2020. Note that the exact location of the site may have been adjusted to ensure that all histograms are included in the map.

with the simulation outcomes. It is worth noting that at Wollongong, O_3 measurements were conducted in January and February 2020, but were halted during March–April, and subsequently resumed in May 2020 with good number of observations. Moreover, O_3 observations at Bremen were very limited to a few observations in March and April and therefore not included in the results. This study provides valuable insights into the significance of combining column and near-surface localized observations. Notably, previous studies have demonstrated that reductions in NO_2 concentrations at European and Chinese urban sites were accompanied by considerable increases in O_3, resulting in a shift from a VOC-limited regime to a NO_x-limited regime (Gaubert et al., 2021; Grange et al., 2021; Liu et al., 2021; Zhang et al., 2022).

3.2. Anomalies of CO, C_2H_2, C_2H_6, and H_2CO in the troposphere

Figure 5 shows the monthly mean time series of CO and the predicted values at Boulder, Colorado. As mentioned before, the forecasting approach works better for gases like CO, which present a significant declining trend in the past decades. The calculated MAPE value of -1.5% indicates good validation at Boulder. All other sites show similar values. **Figure 6** shows the monthly mean observed and predicted 2020 values for the FTIR and the CAM-chem simulations (top) and anomalies (bottom). Typically, CO shows larger values in the winter and early spring due to low concentrations of hydroxyl (OH) radical and minimum levels in autumn, however a second peak enhancement in the early autumn is captured more often due to rising emissions from wildfires over North America (Buchholz et al., 2022). The predicted values also capture this second peak, although the exceptional enhancements measured in 2022 were very large. Between March and May there was a slightly mean negative anomaly of $-1.3\% \pm 2.1\%$, then between May and July anomalies remained the same and between August and October the CO shows significant positive anomalies due to the exceptional wildfires in the region. The magnitude of the CAM-chem anomalies agree quite well with the FTIR observations. At the beginning of the year there was a slightly positive anomaly explained by natural variability, then starting in March COVID-19 started to play a role and the total mean anomaly between March and May is $-2.4\% \pm 0.9\%$.

Figure 7a shows the CO anomalies at all sites between March and May 2020. A decrease in CO is detected in most of the Northern Hemisphere urban sites (Paris, Toronto, Boulder, Tsukuba, and Hefei) with negative values between 1% and 12%. The most substantial reduction in CO levels was recorded in Hefei, China, where there was a decrease of $-11.7\% \pm 6.9\%$. However, it is worth noting that an even more significant decrease was observed in late February 2020, which aligns with the strict lockdowns that were implemented in several Chinese cities during that time (Levelt et al., 2021; Stavrakou et al., 2021). Overall, the CO reductions are captured in the simulations for most of the urban sites. At some sites, the effects of natural variability and COVID-19 impacts are in opposition. For instance, at Boulder and Toronto, the contribution of

Table 5. Summary of tropospheric O_3 mean anomalies[a] during the 2020 stringent COVID-19 lockdown, arranged by latitude for all sites

Station	FTIR (Observed-Predicted) [%]	CAM-chem (Total) [%]	CAM-chem (COVID-19) [%]	CAM-chem (Nat. Variability) [%]
Thule	−14.1 ± 4.1	−12.4 ± 2.6	−2.0 ± 0.9	−10.3 ± 2.4
Kiruna	−7.5 ± 1.9	−5.9 ± 3.5	−2.0 ± 0.8	−3.9 ± 3.4
Jungfraujoch	−14.8 ± 1.6	−15.9 ± 2.6	−3.6 ± 1.4	−12.3 ± 2.2
Toronto	−9.4 ± 3.6	−6.7 ± 2.9	−2.6 ± 1.1	−4.2 ± 2.7
Boulder	−12.7 ± 2.0	−5.2 ± 3.0	−3.6 ± 1.2	−1.7 ± 2.8
Tsukuba	−10.0 ± 2.7	−3.5 ± 2.7	−2.4 ± 1.1	−1.2 ± 2.5
Hefei	−0.1 ± 3.9	−5.9 ± 3.3	−2.6 ± 0.8	−3.4 ± 3.2
Izana	−11.4 ± 0.5	−11.7 ± 1.7	−2.9 ± 1.2	−8.8 ± 1.3
Wollongong	−2.8 ± 0.0	−0.5 ± 0.0	−3.2 ± 0.0	2.7 ± 0.0

FTIR = Fourier-transform infrared spectrometer; CAM-chem = Community Atmosphere Model with chemistry.

[a]Calculated as the mean values of relative differences obtained between March and May 2020. Error bars represent the standard deviation within those months.

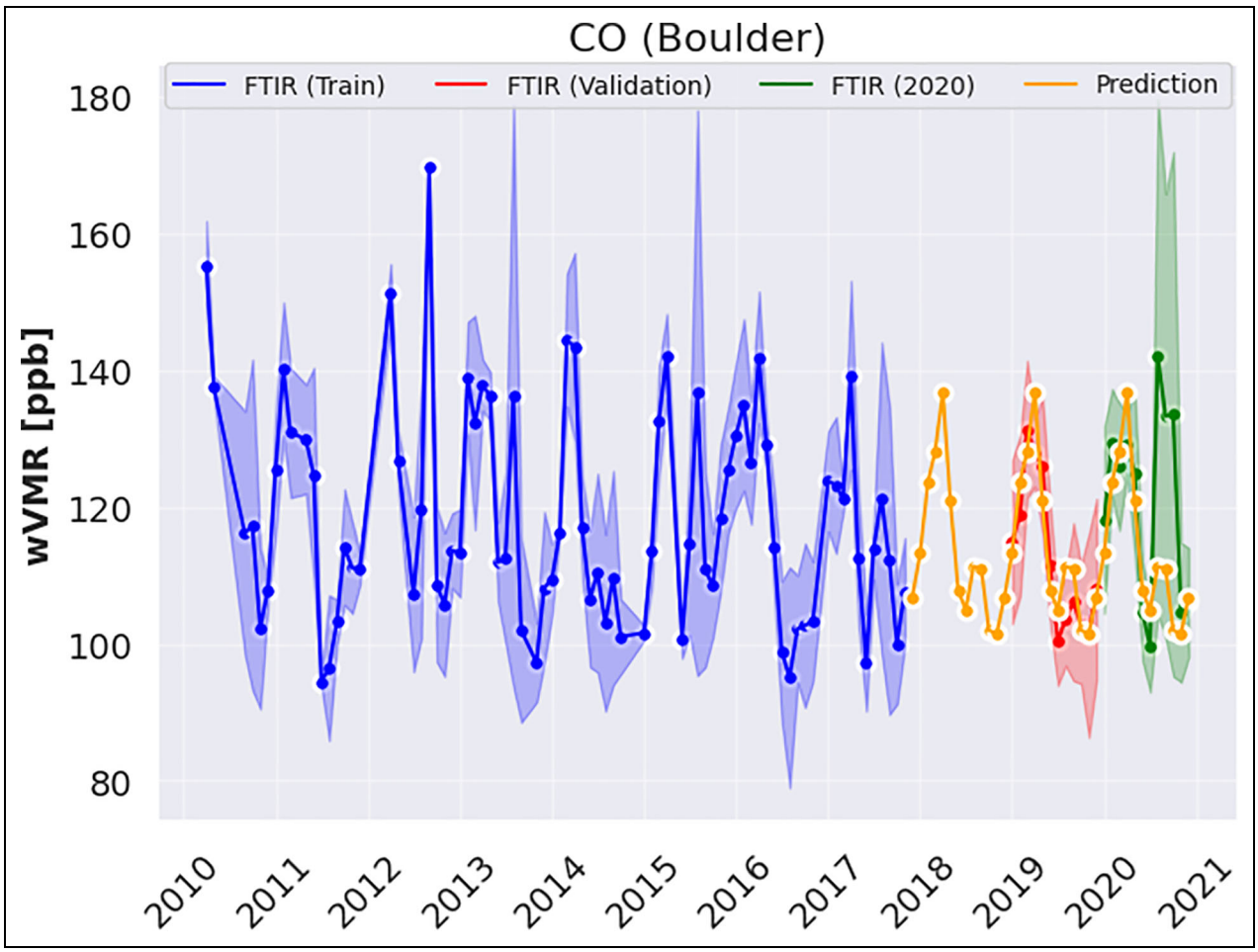

Figure 5. Time series of monthly mean CO weighted volume mixing ratios (wVMR) at Boulder, Colorado. The blue line represents the observations used to train the model and predict 2018–2020 monthly values (orange), which then are assessed in 2019 during the validation period (red) and calculate anomalies during the COVID-19 stringent period in 2020 using actual observations (green). The shaded area represent the standard deviation.

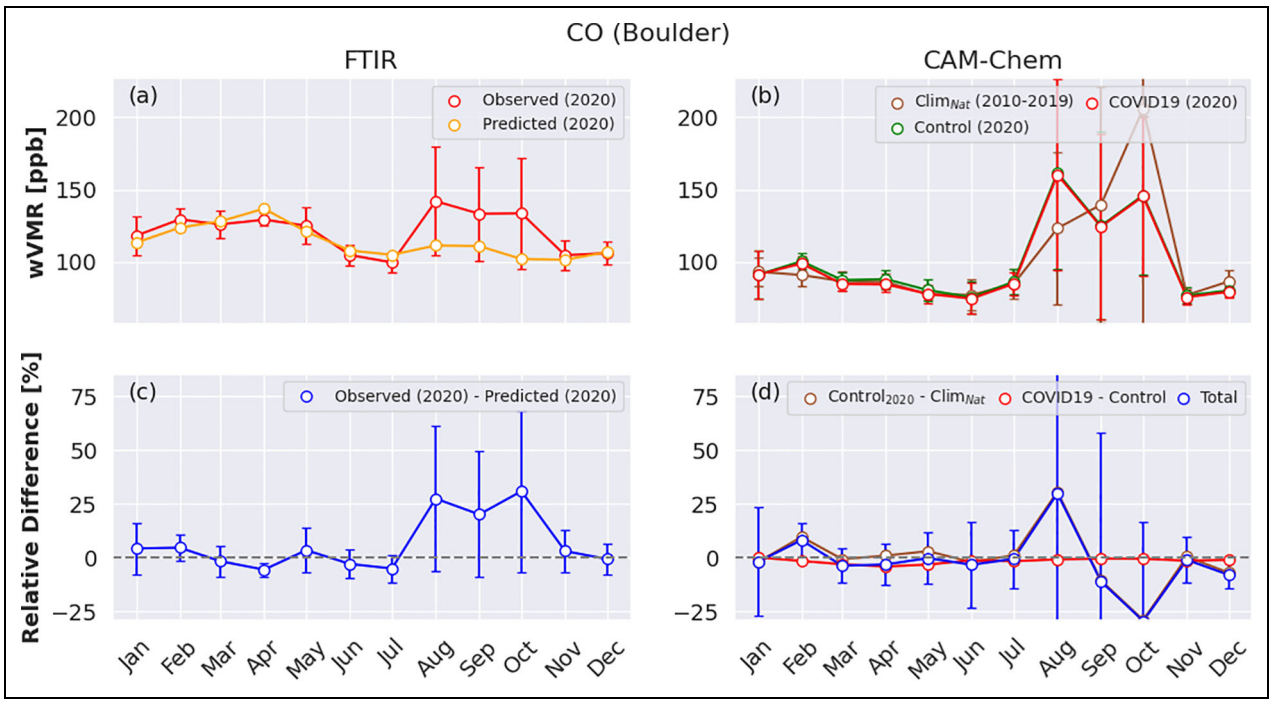

Figure 6. (a) Monthly mean weighted volume mixing ratios (wVMR) of CO observed (red) and predicted business-as-usual in 2020 (orange) at Boulder, Colorado. (b) CAM-chem simulations for the control scenario in 2020 (green), COVID-19 adjusted emission scenario (red), and natural variability climatology simulations (brown). (c) Illustrates the relative differences between the observations and predicted levels for each month in 2020. (d) Relative differences between the COVID-19 and control (red) and between the control and natural variability simulations (brown), with the combined effect of COVID-19 lockdown and natural variability depicted in blue. A comprehensive overview of the various simulations and methods used to obtain them is available in **Table 4**.

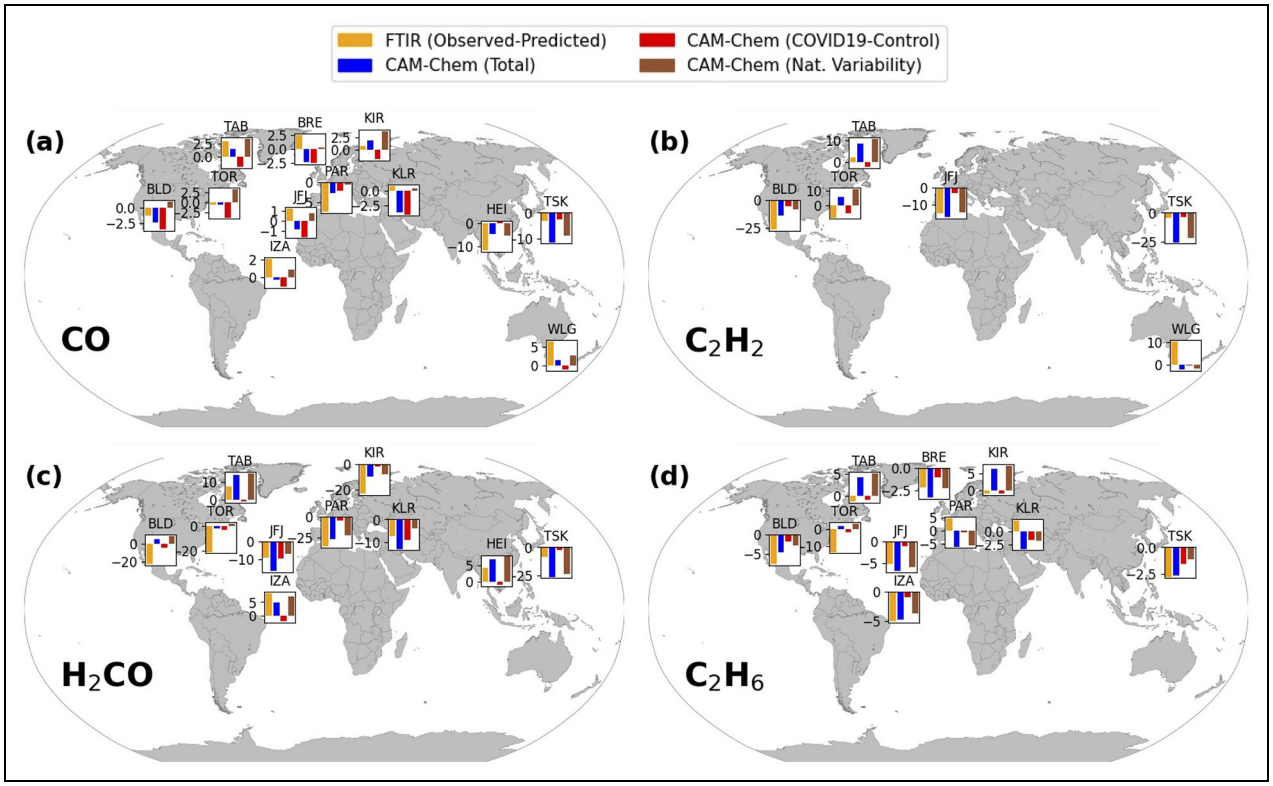

Figure 7. Map with tropospheric anomalies of CO (a), C_2H_2 (b), H_2CO (c), and C_2H_6 (d) at different sites, expressed as a percentage and estimated using mean values obtained between March and May 2020. Note that the exact location of the site may have been adjusted to ensure that all histograms are included in the map.

Table 6. Summary of tropospheric CO mean anomalies[a] during the 2020 stringent COVID-19 lockdown, arranged by latitude for all sites

Station	FTIR (Observed-Predicted) [%]	CAM-chem (Total) [%]	CAM-chem (COVID-19) [%]	CAM-chem (Nat. Variability) [%]
Thule	2.9 ± 1.7	1.5 ± 1.5	−1.9 ± 0.3	3.4 ± 1.5
Kiruna	0.8 ± 0.6	1.9 ± 0.7	−2.0 ± 0.2	4.0 ± 0.6
Bremen	2.5 ± 4.0	−2.3 ± 1.6	−2.5 ± 0.2	0.2 ± 1.6
Karlsruhe	0.7 ± 1.0	−3.6 ± 0.7	−3.9 ± 0.6	0.4 ± 0.4
Paris	−7.5 ± 1.2	−2.6 ± 1.4	−2.0 ± 0.4	−0.6 ± 1.3
Jungfraujoch	1.2 ± 1.2	−0.8 ± 1.3	−1.6 ± 0.2	0.7 ± 1.3
Toronto	−0.6 ± 0.7	−0.7 ± 1.0	−3.9 ± 0.4	3.2 ± 0.9
Boulder	−1.3 ± 2.1	−2.4 ± 0.9	−3.5 ± 0.3	1.1 ± 0.9
Tsukuba	−3.1 ± 2.1	−11.3 ± 4.9	−2.5 ± 0.1	−8.8 ± 4.9
Hefei	−11.7 ± 6.9	−4.7 ± 3.6	0.5 ± 1.4	−5.3 ± 3.3
Izana	2.1 ± 3.9	−0.3 ± 1.6	−1.1 ± 0.2	0.8 ± 1.6
Wollongong	6.5 ± 0.2	1.6 ± 0.9	−1.1 ± 0.0	2.7 ± 0.9

FTIR = Fourier-transform infrared spectrometer; CAM-chem = Community Atmosphere Model with chemistry.

[a]Calculated as the mean values of relative differences obtained between March and May 2020. Error bars represent the standard deviation within those months.

natural variability indicates an increase. Based on the simulations, the natural variability does not seem to have a significant impact on most of the urban European sites. The decrease in Paris is explained only by COVID-19 reductions, although observations were limited at the beginning and in the middle of the confinement. The CO anomaly in Karlsruhe does not show a significant change and Bremen saw an increase, although measurements were limited only to some days in March and April. In Hefei, the decrease in CO is further amplified by natural variability. Interestingly, the remote sites (Thule, Izaña, Jungfraujoch, and Kiruna) show a slight increase between 1% and 3%. The overall increase in these remote sites is captured by the simulations. Wollongong, the only Southern Hemisphere site, shows an increase of 6.5% in the observations that can be linked to the Australian fires around December 2019 and January 2020 (Salawitch and McBride, 2022). CAM-chem captures the increase but it is underestimated. The natural variability run with repeated emissions have the 2020 fires but not the 2019 ones, which may explain the underestimation. A summary of the CO anomalies among the different sites and CAM-chem simulations is provided in **Table 6**.

To further understand global CO changes we use the long-term record of the Measurements of Pollution in the Troposphere (MOPITT) instrument, aboard the National Aeronautics and Space Administration Terra satellite, to capture global anomalies of CO from space. The MOPITT instrument and the retrieval algorithm are described in detail elsewhere (Drummond et al., 2010; Worden et al., 2013). Briefly, we use the recent version 9 joint thermal-infrared and near-infrared and applied the forecasting approach to the gridded monthly mean total columns data set (2005–2018) to produce business-as-usual values in 2019 and 2020. Similarly, 2019 is used to evaluate the model. **Figure 8** shows CO global anomalies obtained for March (a) and between March and May (b) 2020. CO anomalies vary across regions and they are sensitive to regional and continental scales but overall the Northern Hemisphere shows a decrease while the Southern Hemisphere shows an increase. The overall decrease of CO in the Northern Hemisphere was larger in March 2020 and there is a slow down in the decrease toward May. Disentangling the possible COVID-19 lockdown signal from other causes such as large day-to-day variability, long-range transport, emissions, and chemistry is challenging for CO. The comparison of monthly mean anomalies between MOPITT and FTIR is shown in the supplement (Figure S1). Even though the instruments may sample different spatial scales and sample at different times there is a high level of consistency in the anomalies.

Figure 7 also shows anomalies of C_2H_2, H_2CO, and C_2H_6 for all sites. Although a limited number of sites retrieve C_2H_2 there is a drop of −26.2%, −8.1%, and −4.6% for the urban Northern Hemisphere sites Boulder, Toronto, and Tsukuba, respectively. Jungfraujoch, a remote site, also shows a significant decrease of −15.4%. The magnitude of the anomaly is well captured at Jungfraujoch, however, all other sites show a significant bias between observed and modeled anomalies. Note that although the magnitude of the anomalies is not fully captured with CAM-chem simulations there is an agreement in the decrease for Boulder and Tsukuba, likely related to reductions in combustion emissions (Xiao et al., 2007). There is an increase of C_2H_2 at Wollongong, which is likely related with the Australian fires identified

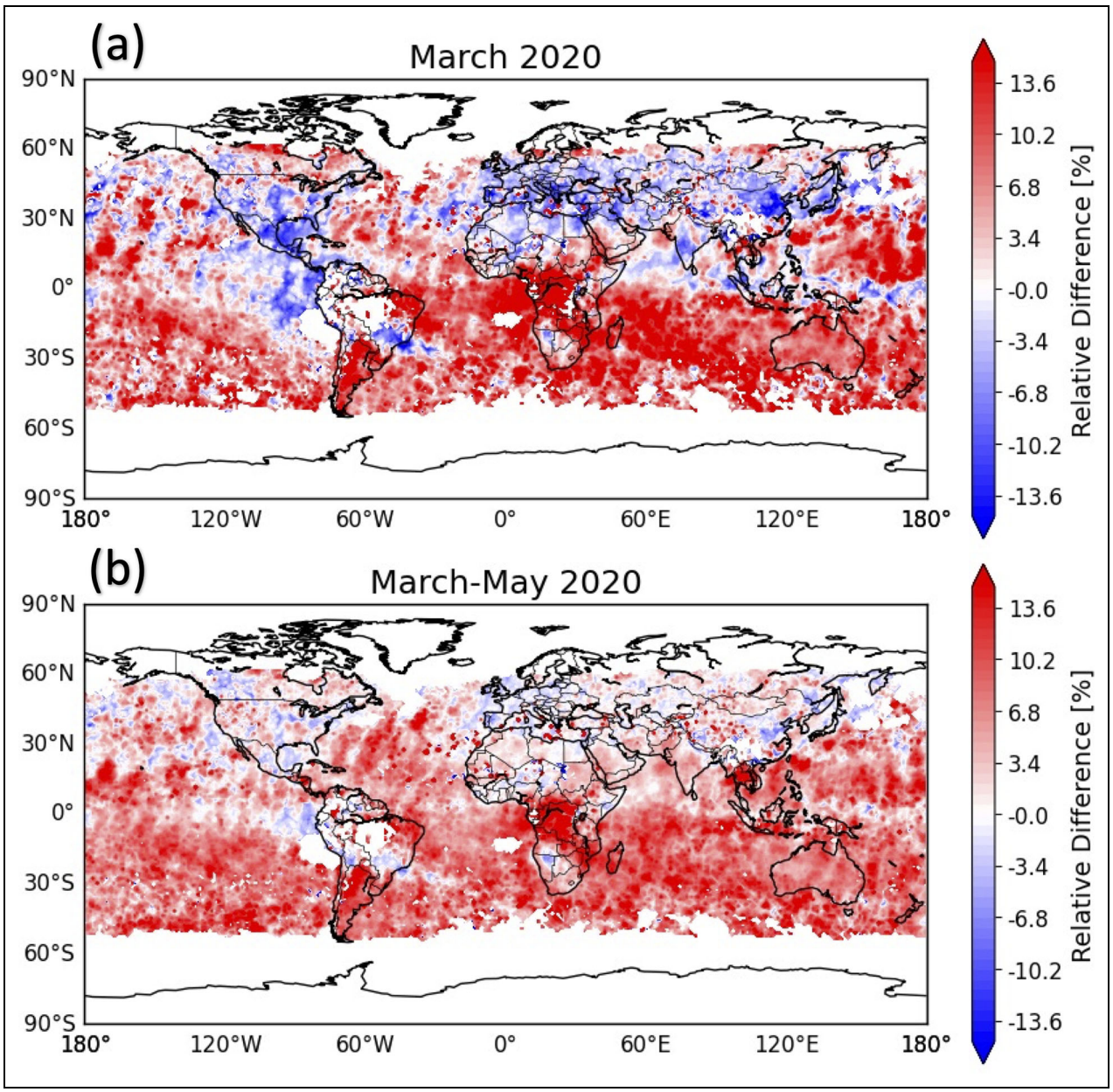

Figure 8. CO anomalies obtained with MOPITT global observations in March (a) and between March and May (b) 2020.

at the end of 2019 and early 2020. We believe that the role of natural variability such as transport is expected to be more important for species with shorter lifetime such as C_2H_2. Except for a few sites (Thule, Izaña, and Hefei) the H_2CO anomalies are also negative and in most cases simulations agree well, however, in some cases there is a significant bias. At Hefei, the mean anomaly is positively skewed by 4.3% ± 12.0% and is largely influenced by a noteworthy rise in H_2CO levels in May. However, there was a noticeable drop of approximately 50% in February, which aligns with the findings of Levelt et al. (2021), where they observed a 40% decline of H_2CO in late February 2020 using satellite observations. CAM-chem simulations show that H_2CO decreased due to the the strict lockdown period but the magnitude of the natural variability is larger for all sites, likely dominating the variability. C_2H_6 shows large variability and we identify a decline during the stringent 2020 lockdown for some urban sites (Toronto, Boulder) but others show an increase (Paris, Karlsruhe). Similar to H_2CO, simulations show small changes in C_2H_6 due to COVID-19 restrictions but rather large variability due to natural variability. Although the CAM-chem simulations provide reasonable estimations of the anomalies observed in C_2H_2, H_2CO, and C_2H_6, it remains difficult to accurately assess the extent to which the COVID-19 lockdowns impacted these gases. The simulations suggest that natural variability, including meteorological factors, fluctuations in biogenic emissions, and occurrences of biomass burning events, played a significant role in the changes observed in 2020. The results for all sites are shown in **Tables 7**, **8**, and **9** for C_2H_2, H_2CO, and C_2H_6, respectively.

Table 7. Summary of tropospheric C_2H_2 mean anomalies[a] during the 2020 stringent COVID-19 lockdown, arranged by latitude for all sites

Station	FTIR (Observed-Predicted) [%]	CAM-chem (Total) [%]	CAM-chem (COVID-19) [%]	CAM-chem (Nat. Variability) [%]
Thule	2.1 ± 10.0	8.6 ± 5.5	−2.3 ± 0.3	10.9 ± 5.5
Jungfraujoch	−15.4 ± 1.7	−17.6 ± 3.5	−2.9 ± 0.4	−14.7 ± 3.5
Toronto	−8.1 ± 4.1	5.9 ± 4.1	−5.0 ± 0.5	10.9 ± 4.1
Boulder	−26.2 ± 2.0	−13.9 ± 5.6	−5.8 ± 0.5	−8.1 ± 5.6
Tsukuba	−4.6 ± 4.4	−25.7 ± 14.7	−4.0 ± 0.5	−21.7 ± 14.7
Wollongong	10.4 ± 8.8	−2.4 ± 2.9	−0.6 ± 0.3	−1.8 ± 2.8

FTIR = Fourier-transform infrared spectrometer; CAM-chem = Community Atmosphere Model with chemistry.

[a]Calculated as the mean values of relative differences obtained between March and May 2020. Error bars represent the standard deviation within those months.

Table 8. Summary of tropospheric H_2CO mean anomalies[a] during the 2020 stringent COVID-19 lockdown, arranged by latitude for all sites

Station	FTIR (Observed-Predicted) [%]	CAM-chem (Total) [%]	CAM-chem (COVID-19) [%]	CAM-chem (Nat. Variability) [%]
Thule	7.6 ± 4.8	14.1 ± 4.8	−1.1 ± 0.5	15.1 ± 4.7
Kiruna	−23.2 ± 5.3	−9.9 ± 9.6	−1.8 ± 0.6	−8.1 ± 9.6
Karlsruhe	−7.5 ± 4.5	−13.0 ± 4.9	−8.9 ± 1.7	−4.1 ± 4.6
Paris	−36.0 ± 23.5	−27.0 ± 24.0	−4.4 ± 3.5	−22.6 ± 23.7
Jungfraujoch	−9.3 ± 7.6	−16.8 ± 3.7	−9.7 ± 2.3	−7.1 ± 3.0
Toronto	−21.1 ± 4.3	−2.1 ± 8.5	−3.6 ± 1.0	1.5 ± 8.4
Boulder	−22.9 ± 8.2	5.2 ± 7.8	−4.0 ± 0.9	9.2 ± 7.8
Tsukuba	−8.2 ± 18.7	−25.9 ± 9.6	−2.5 ± 0.5	−23.4 ± 9.6
Hefei	4.3 ± 12.0	6.9 ± 1.4	−0.9 ± 0.8	7.8 ± 1.2
Izana	8.4 ± 5.7	4.9 ± 2.2	−2.2 ± 0.8	7.1 ± 2.0

FTIR = Fourier-transform infrared spectrometer; CAM-chem = Community Atmosphere Model with chemistry.

[a]Calculated as the mean values of relative differences obtained between March and May 2020. Error bars represent the standard deviation within those months.

To quantify anomalies, the relative difference is calculated as the fraction of the difference between actual observations and the predicted 2020 divided by the predicted value itself. This is illustrated in the bottom plots.

3.3. Anomalies of O_3 and CO in the UTLS

Figure 9 shows anomalies of O_3 and CO in the UTLS obtained with both FTIRs and CAM-chem simulations. A summary of the anomalies along with the contributions from CAM-chem simulations are shown in **Tables 10** and **11** for O_3 and CO, respectively. All observations in North America and Europe detected large drops of O_3 in the UTLS with the largest reduction in Thule (−28.7% ± 9.3%) partially due to the record-low springtime Arctic O_3 values as discussed in the next section. CAM-chem simulations agree well with observations. Reduced surface emissions during the COVID-19 lockdown did not have a significant impact on the reduction observed, as natural variability played a more important role. The reduction in O_3 levels in the upper troposphere is consistent with the findings of Clark et al. (2021), who observed a decrease in O_3 in the free troposphere around Frankfurt airport. Additionally, Reifenberg et al. (2022) found substantial negative relative changes in the upper troposphere for certain species over Europe using numerical simulations, which included a decrease in NO_x due to reduced air traffic during the lockdown period (Bouarar et al., 2021; Nussbaumer et al., 2022). Tsukuba is the only site with an increase in O_3 in the UTLS explained by the fact that Tsukuba was not affected by the low O_3 contribution from the stratosphere as pointed out in **Table 12**. Bremen and Hefei are not shown because the forecasting approach shows MAPE

Table 9. Summary of tropospheric C_2H_6 mean anomalies[a] during the 2020 stringent COVID-19 lockdown, arranged by latitude for all sites

Station	FTIR (Observed-Predicted) [%]	CAM-chem (Total) [%]	CAM-chem (COVID-19) [%]	CAM-chem (Nat. Variability) [%]
Thule	−1.2 ± 4.8	4.4 ± 3.4	−0.9 ± 0.2	5.3 ± 3.4
Kiruna	−0.9 ± 0.7	6.4 ± 0.6	−0.9 ± 0.2	7.2 ± 0.5
Bremen	−2.1 ± 1.1	−3.2 ± 2.2	−1.0 ± 0.1	−2.2 ± 2.2
Karlsruhe	2.0 ± 1.6	−3.3 ± 1.8	−1.6 ± 0.3	−1.8 ± 1.8
Paris	4.5 ± 0.3	−5.9 ± 5.2	−0.5 ± 0.2	−5.5 ± 5.2
Jungfraujoch	−5.1 ± 2.4	−6.8 ± 2.3	−1.0 ± 0.4	−5.9 ± 2.3
Toronto	−13.8 ± 0.9	1.9 ± 1.5	−1.5 ± 0.2	3.4 ± 1.5
Boulder	−7.6 ± 4.3	−4.6 ± 1.3	−1.8 ± 0.2	−2.8 ± 1.3
Tsukuba	−2.8 ± 4.9	−2.7 ± 2.0	−1.5 ± 0.1	−1.1 ± 2.0
Izana	-5.0 ± 10.7	−4.7 ± 3.5	−0.9 ± 0.1	−3.7 ± 3.5

FTIR = Fourier-transform infrared spectrometer; CAM-chem = Community Atmosphere Model with chemistry.

[a]Calculated as the mean values of relative differences obtained between March and May 2020. Error bars represent the standard deviation within those months.

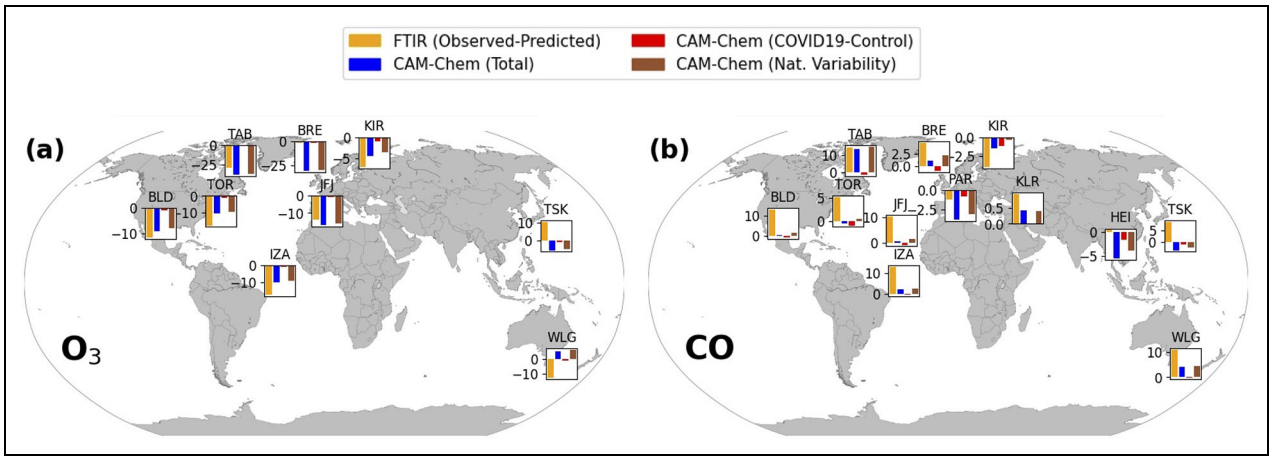

Figure 9. Map with tropospheric anomalies of O_3 (a) and CO (b) in the upper tropospheric and lower stratosphere (UTLS) at different sites, expressed as a percentage and estimated using mean values obtained between March and May 2020. Note that the exact location of the site may have been adjusted to ensure that all histograms are included in the map.

values larger than 20%. Wollongong O_3 measurements only occurred in May and show a decrease in O_3 but it is hard to pinpoint the reason. The majority of sites indicate a significant positive anomaly of CO in the UTLS. CAM-chem does not capture well the magnitude of the anomalies indicating an extra cause not studied in this model simulation. We will further discuss the role of chemistry in the next sections.

3.4. Ozone stratospheric-tropospheric transport changes in 2020

The tagged stratospheric O_3 in the simulations is used to evaluate the difference of the stratospheric contribution into the troposphere in 2020 with respect to the long-term simulations (2010–2019). In order to quantify the typical contribution of stratospheric O_3 into the troposphere, the ratio of tagged stratospheric O_3 to total O_3 is calculated for 2010–2019. Similarly, the ratio is calculated using the tagged 2020 stratospheric O_3 and the total 2010–2019 climatology. As an example, **Figure 10a** shows the ratios for Thule, Greenland, which was directly situated below the O_3 depletion in 2020 (Manney et al., 2020). Under normal conditions, the downward contribution of ozone-rich air from the stratosphere starts to decrease at 9 km reaching around 50% at the surface (blue line). In 2020 (green line), the contribution is lower for all altitudes below 20 km. The relative difference (**Figure 10b**) shows that the major decrease in the

Table 10. Summary of UTLS O_3 mean anomalies[a] during the 2020 stringent COVID-19 lockdown, arranged by latitude for all sites

Station	FTIR (Observed-Predicted) [%]	CAM-chem (Total) [%]	CAM-chem (COVID-19) [%]	CAM-chem (Nat. Variability) [%]
Thule	−28.7 ± 9.3	−37.4 ± 7.2	−1.2 ± 0.4	−36.2 ± 7.2
Kiruna	−6.9 ± 6.3	−4.4 ± 5.9	−0.9 ± 0.4	−3.6 ± 5.8
Jungfraujoch	−13.9 ± 2.0	−17.2 ± 2.4	−1.0 ± 0.4	−16.2 ± 2.3
Toronto	−18.0 ± 7.2	−10.5 ± 6.5	−1.1 ± 0.5	−9.5 ± 6.5
Boulder	−11.5 ± 3.5	−9.0 ± 8.0	−1.0 ± 0.4	−8.0 ± 8.0
Tsukuba	10.2 ± 7.4	−5.6 ± 4.5	−0.8 ± 0.4	−4.7 ± 4.5
Izana	−17.1 ± 1.5	−9.7 ± 1.3	−0.8 ± 0.3	−8.9 ± 1.3
Wollongong	−12.8 ± 0.0	5.5 ± 0.0	−1.0 ± 0.0	6.5 ± 0.0

FTIR = Fourier-transform infrared spectrometer; CAM-chem = Community Atmosphere Model with chemistry; UTLS = upper tropospheric and lower stratosphere.

[a]Calculated as the mean values of relative differences obtained between March and May 2020. Error bars represent the standard deviation within those months.

Table 11. Summary of UTLS CO mean anomalies[a] during the 2020 stringent COVID-19 lockdown, arranged by latitude for all sites

Station	FTIR (Observed-Predicted) [%]	CAM-chem (Total) [%]	CAM-chem (COVID-19) [%]	CAM-chem (Nat. Variability) [%]
Thule	14.9 ± 9.0	13.8 ± 4.9	−1.6 ± 0.3	15.3 ± 4.9
Kiruna	−3.9 ± 1.7	−1.5 ± 3.3	−1.2 ± 0.2	−0.3 ± 3.3
Bremen	4.5 ± 4.1	1.1 ± 0.3	−0.9 ± 0.1	2.1 ± 0.3
Karlsruhe	0.9 ± 1.0	0.4 ± 0.5	0.0 ± 0.2	0.4 ± 0.4
Paris	−1.3 ± 7.0	−3.9 ± 5.6	−0.7 ± 0.2	−3.2 ± 5.6
Jungfraujoch	10.3 ± 0.8	0.5 ± 1.9	−0.9 ± 0.1	1.4 ± 1.9
Toronto	5.2 ± 4.4	−0.5 ± 2.3	−1.0 ± 0.0	0.5 ± 2.3
Boulder	13.4 ± 3.7	0.3 ± 1.9	−1.0 ± 0.1	1.2 ± 1.9
Tsukuba	8.5 ± 5.5	−3.6 ± 1.5	−1.1 ± 0.2	−2.5 ± 1.5
Hefei	0.3 ± 0.6	−5.4 ± 4.1	−1.6 ± 0.7	−3.8 ± 4.1
Izana	13.1 ± 1.0	2.4 ± 0.8	−0.4 ± 0.2	2.7 ± 0.8
Wollongong	11.0 ± 2.7	4.1 ± 2.6	−0.3 ± 0.0	4.4 ± 2.6

FTIR = Fourier-transform infrared spectrometer; CAM-chem = Community Atmosphere Model with chemistry; UTLS = upper tropospheric and lower stratosphere.

[a]Calculated as the mean values of relative differences obtained between March and May 2020. Error bars represent the standard deviation within those months.

stratospheric contribution in 2020 occurred at 10 km (about −45%). Overall, the mean decrease contribution in the troposphere is 13.3%. The same analysis is carried out for all sites and results of changes in the contribution of ozone-rich air from the stratosphere are shown in **Table 12**. Results are consistent with respect to the location of each site, for example, northern high latitude sites (Thule, Kiruna, and Jungfraujoch) show the highest decrease in the contribution of ozone-rich air from the stratosphere to the troposphere.

3.5. Implication for CH_4 lifetime

We found a mostly neutral CO signal to COVID-19 restrictions despite emission reductions that include anthropogenic CO precursors, as reflected by H_2CO observation anomalies. **Figure 11** shows CAM-chem anomalies of the

Table 12. Summary of the mean change of O_3 stratospheric contribution into the troposphere in 2020 (compared to 2010–2019), in percent and standard deviation, calculated between March and May 2020 for all sites arranged by latitude

Station	Relative Change [%]
Thule	−13.3 ± 1.8
Kiruna	−5.5 ± 2.9
Bremen	−0.1 ± 2.2
Jungfraujoch	−9.7 ± 4.8
Toronto	−1.8 ± 1.9
Boulder	−5.0 ± 1.9
Tsukuba	2.2 ± 1.7
Hefei	0.9 ± 2.7
Izana	−2.2 ± 2.3
Wollongong	10.4 ± 3.5

CH_4 and CO lifetime with respect to their chemical loss in the atmosphere. The net emission reduction impact suggests a decrease in global tropospheric OH by more than 2%, starting in April and for the rest of the year. The negative OH anomalies were particularly large for April, May, and June, and our model estimates net positive anomalies in the lifetimes of CH_4 and CO of 2%–3% for these 3 months. Interestingly, the net anomalies for 2020 were nearly neutral for the last 6 months of 2020, because of equally large natural anomalies. We performed an additional simulation with only reduction in anthropogenic NO_x emissions, for both aircraft and the surface fluxes. This leads to a larger peak in CH_4 lifetime anomalies, roughly 5% instead of 4% for the lockdowns effects only, which would translate into an additional 20% increase in CH_4 growth rate for that month. This provides model confirmation that emission reduction of NMVOCs and CO tends to mitigate the NO_x impact on OH, as recently reviewed by Akimoto and Tanimoto (2022) and characterized in, for example, chemical reanalyses (Gaubert et al., 2017). Recently, Peng et al. (2022) also shows that OH decreased significantly compared to 2019, in

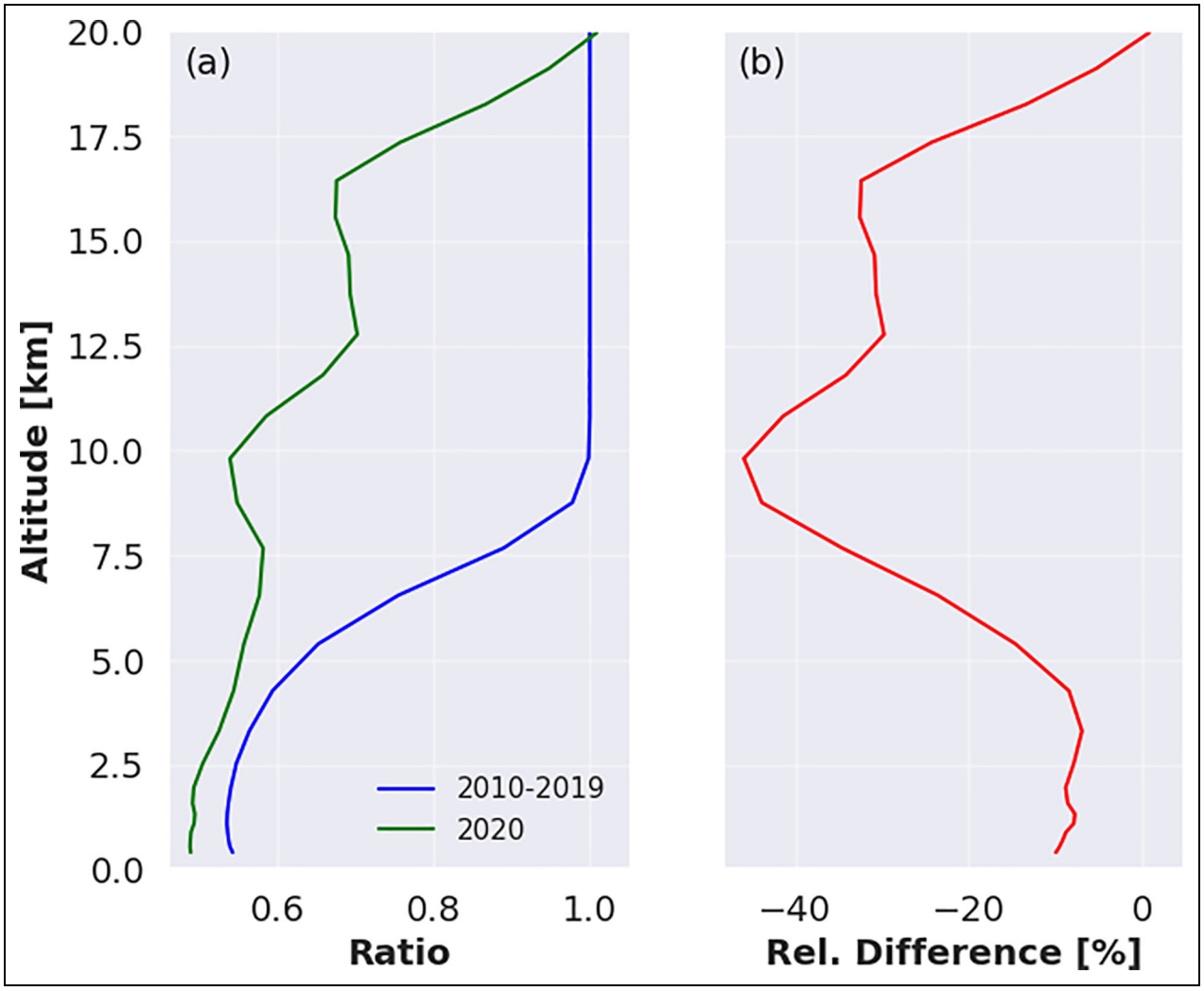

Figure 10. (a) Mean altitude profile ratios of stratospheric tagged O_3 for 2010–2019 (blue) and 2020 (green) to total O_3 profiles calculated between the months of March and May. (b) Relative difference between the typical ratio (2010–2019) and 2020. This is an example for Thule, Greenland.

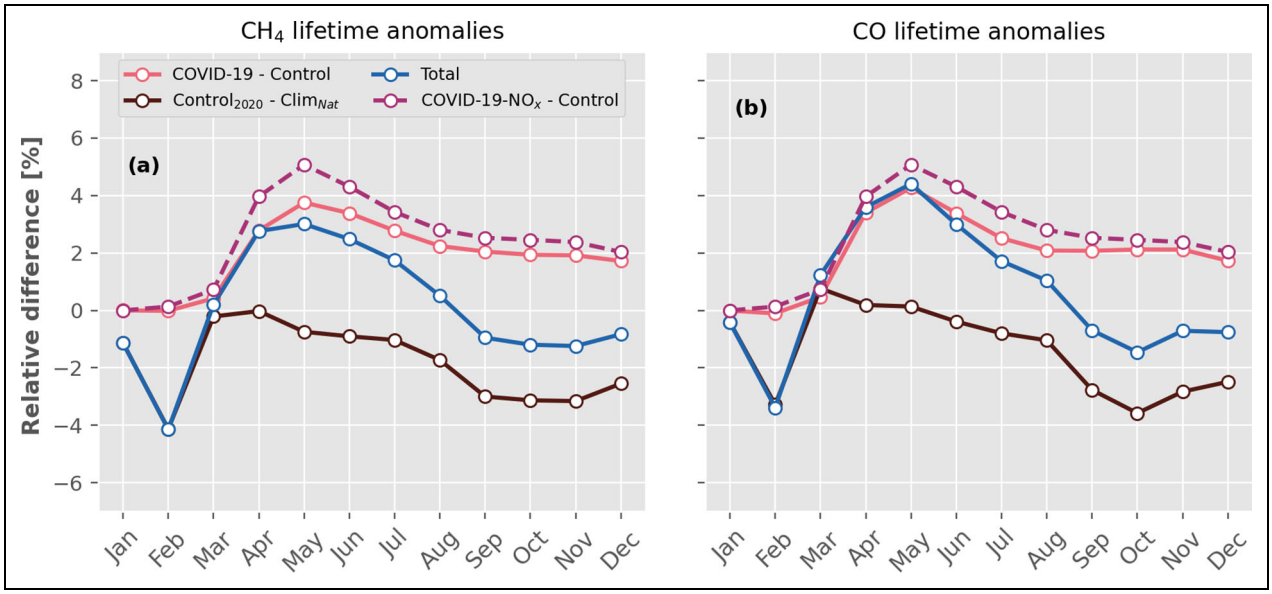

Figure 11. 2020 monthly relative anomalies (%) of the global and tropospheric CH_4 (a) and CO (b) lifetime.

addition to an increase in wetland CH_4 emissions. By contrasting CO observations and model simulation with comprehensive chemistry, we can directly assess the 2020 chemical anomalies.

3.6. Summary and conclusions

The stringent restrictions in anthropogenic activities associated with the world-wide COVID-19 2020 pandemic represented a unique opportunity to study changes in atmospheric composition. In this work, we conducted an analysis of several gases (O_3, CO, C_2H_2, H_2CO, and C_2H_6) and report changes (anomalies) during the strongest COVID-19 2020 lockdown using multiple ground-based FTIRs in both urban (or semi-urban) and remote locations. Here, we utilized a forecasting approach to the observations to predict 2020 business-as-usual tropospheric columns. This involved analyzing long-term records to capture trends and interannual variability. By comparing these predicted values with actual observations, we calculated monthly mean anomalies for the year 2020. In this work, we emphasized results from the strict COVID-19 period in 2020 (March–May). Interpreting anomalies solely from observations is a challenging task because natural variability, chemistry, and photochemical regimes may play an important role. To gain a better understanding of these changes, we employed global CAM-chem simulations dedicated to disentangle the role of COVID-19 stay-at-home restrictions and natural variability on these gases.

Out of all the gases analyzed, O_3 displayed the most consistent tropospheric column negative anomalies with a drop of about 9% between March and May 2020 among all sites. The magnitudes of the observed anomalies are well captured by the model, in particular for remote sites in the Northern Hemisphere, where the natural variability played a significant role, often larger than COVID-19 lockdowns. Quantitative analysis of tagged stratospheric O_3 in the CAM-chem simulations indicates that reductions of the contribution of ozone-rich air from the stratosphere contributed to some of the total tropospheric reduction, especially sites situated below the O_3 depletion, but is not the only reason.

The atmospheric CO signals are more challenging to address because of a delicate balance between emissions, chemical sink, and large natural variability. As expected, urban sites, mainly in the Northern Hemisphere, show reductions ranging between 1% and 12% in tropospheric CO in March–May 2020. In contrast, most remote sites show a small increase, although the magnitude is within uncertainty values. To further characterize the spatial distribution of CO changes, we used the MOPITT satellite instrument to quantify world-wide CO anomalies. Overall we detected reductions in CO close to the source: in China, North America, and Europe in March 2020. However, the lack of reduction signals, in April, May, and June, suggests an increase in CO lifetime due to a reduced OH caused by reduced NO_x emissions. Our derived CH_4 and CO lifetime anomalies suggest a decrease in OH by around 3% for these months, but OH was near neutral for the rest of the year, with the COVID-19 effect being compensated by natural variability. We conclude that it is essential to quantify natural variability and to combine comprehensive chemistry with CH_4 emission simulations to attribute the various contributions to the CH_4 growth rate.

Evaluating worldwide anomalies of C_2H_2, H_2CO, and C_2H_6 from FTIR observations presents certain challenges, primarily due to the limited number of FTIR sites globally and a lower number of sites that retrieve these gases, specifically C_2H_2. Additionally, significant year-to-year interannual differences, variations in biogenic emissions, and occurrences of biomass burning events make it difficult to draw definitive conclusions. Nevertheless, we identified negative anomalies of C_2H_2 for the urban Northern Hemisphere sites Boulder, Toronto, and Tsukuba. The observed anomaly at Wollongong, the only Southern Hemisphere site, is positive (same as CO) and likely related

with the Australian fires identified at the end of 2019 and early 2020 (Salawitch and McBride, 2022). C_2H_6 shows a decline during the stringent 2020 lockdown for some urban sites (Toronto, Boulder, and Tsukuba) but others show an increase (Paris, Karlsruhe). H_2CO also shows negative anomalies for most sites, except for a few sites (Thule, Izaña, and Hefei). CAM-chem simulations show that natural variability is larger than reductions related with COVID-19 for these gases. In general, simulations reproduce the sign of the anomalies but in many cases the bias between observations and simulations is significant and related with uncertainty in emissions during the COVID-19 lockdowns. Our study is expected to serve as a valuable reference within the observational FTIR community, particularly given the significance of rapid changes and anomalous events in atmospheric composition occurring over a short period of time (weeks to months).

The majority of studies examining the impact of the global COVID-19 pandemic on atmospheric composition concentrate solely on changes in the lower troposphere. Conversely, only a limited number of studies have investigated the free troposphere or layers above. A key advantage of utilizing ground-based FTIR instruments is their heightened vertical sensitivity for certain species. Our findings demonstrate the potential to infer changes in O_3 and CO within UTLS. The reductions observed in O_3 were even more substantial within the UTLS, and stratospheric-tropospheric transport contributions were notably smaller than those observed during long-term normal conditions. Regarding CO, UTLS anomalies indicate an increase, and this, along with the slow down in the decrease of tropospheric CO may be related to changes in the CO lifetime.

Data accessibility statement

The data used in this publication were obtained as part of the Network for the Detection of Atmospheric Composition Change (NDACC) and are available through the NDACC website (www.ndacc.org). CESM2.2.0 is a publicly released version of the Community Earth System Model and freely available online (at www.cesm.ucar.edu). The CAM-chem simulations are available for download online (Gaubert et al., 2023).

Supplemental material

The supplemental files for this article can be found as follows:

Figure S1.

Acknowledgments and Funding

This material is based upon work supported by the National Center for Atmospheric Research (NCAR), which is a major facility sponsored by the National Science Foundation under Cooperative Agreement No. 1852977. This study has been supported under contract by the National Aeronautics and Space Administration (NASA) award No. NNX17AE38G. We would like to acknowledge the high-performance computing support from Cheyenne Computational and Information Systems Laboratory (2019) provided by NCAR's Computational and Information Systems Laboratory of the National Center for Atmospheric Research (NCAR), sponsored by the US National Science Foundation (NSF). The MOPITT team acknowledges the contributions of COMDEV and ABB BOMEM with support from the Canadian Space Agency (CSA), the Natural Sciences and Engineering Research Council (NSERC), and Environment Canada. The NCAR MOPITT project is supported by the National Aeronautics and Space Administration (NASA) Earth Observing System (EOS) program. FTIR operation at Tsukuba site is supported in part by the GOSAT series project. The FTIR stations Bremen, Izaña, Karlsruhe, and Kiruna have been supported by the German Bundesministerium für Wirtschaft und Energie (BMWi) via DLR under grants 50EE1711A and B. The Paris TCCON site has received funding from Sorbonne Université, the French research center CNRS, the French space agency CNES, and Région Île-de-France. The ULiège contribution to this work has been supported by the Fonds de la Recherche Scientifique (F.R.S.–FNRS, Brussels, Belgium; grant no. J.0126.21) and the GAW-CH program of MeteoSwiss (Zürich, CH). EM is a senior research associate with F.R.S.–FNRS. The ULiège team thanks the International Foundation High Altitude Research Stations Jungfraujoch and Gornergrat (HFSJG, Bern, CH) for supporting the facilities needed to perform the Fourier transform infrared observations at Jungfraujoch. The Toronto FTIR measurements were made at the University of Toronto Atmospheric Observatory, primarily supported by the Natural Sciences and Engineering Research Council of Canada and Environment and Climate Change Canada.

Competing interests

The authors declare no competing financial interests.

Author contributions

Contributed to conceptualization, methodology, investigation, analysis, writing—review and editing: IO.

Contributed to CAM-chem simulations, software, investigation, writing—review and editing: BG.

Contributed to investigation, methodology, supervision, writing—review and editing: JWH.

Contributed to conceptualization, review and editing: GB.

Contributed to MOPITT analysis, review and editing: HMW.

Contributed with ground-based FTIR data and review: TB, HF, FH, PJ, NJ, CL, EM, IMo, IMu, JN, MP, AR, YT, KS, YS, SY.

References

Addas, A, **Maghrabi, A.** 2021. The impact of COVID-19 lockdowns on air quality–A global review. *Sustainability* **13**(18). DOI: http://dx.doi.org/10.3390/su131810212. Available at https://www.mdpi.com/2071-1050/13/18/10212.

Akimoto, H, **Tanimoto, H.** 2022. Rethinking of the adverse effects of NO_x-control on the reduction of methane and tropospheric ozone—Challenges toward a denitrified society. *Atmospheric Environment* **277**: 119033. DOI: http://dx.doi.org/10.1016/j.atmosenv.2022.119033.

Albores, I, **Buchholz, R**, **Ortega, I**, **Emmons, L**, **Hannigan, J**, **Lacey, F**, **Pfister, G**, **Tang, W**, **Worden, HM**.

2023. Continental-scale atmospheric impacts of the 2020 western U.S. wildfires. *Atmospheric Environment* **294**: 119436. DOI: http://dx.doi.org/10.1016/j.atmosenv.2022.119436. Available at https://www.sciencedirect.com/science/article/pii/S1352231022005015.

Bouarar, I, **Gaubert, B**, **Brasseur, GP**, **Steinbrecht, W**, **Doumbia, T**, **Tilmes, S**, **Liu, Y**, **Stavrakou, T**, **Deroubaix, A**, **Darras, S**, **Granier, C**, **Lacey, F**, **Müller, J-F**, **Shi, X**, **Elguindi, N**, **Wang, T**. 2021. Ozone anomalies in the free troposphere during the COVID-19 pandemic. *Geophysical Research Letters* **48**(16): e2021GL094204. DOI: http://dx.doi.org/10.1029/2021GL094204.

Buchholz, RR, **Park, M**, **Worden, HM**, **Tang, W**, **Edwards, DP**, **Gaubert, B**, **Deeter, MN**, **Sullivan, T**, **Ru, M**, **Chin, M**, **Levy, RC**, **Zheng, B**, **Magzamen, S**. 2022. New seasonal pattern of pollution emerges from changing North American wildfires. *Nature Communications* **13**(1). DOI: http://dx.doi.org/10.1038/s41467-022-29623-8.

Buchholz, RR, **Worden, HM**, **Park, M**, **Francis, G**, **Deeter, MN**, **Edwards, DP**, **Emmons, LK**, **Gaubert, B**, **Gille, J**, **Martínez-Alonso, S**, **Tang, W**, **Kumar, R**, **Drummond, JR**, **Clerbaux, C**, **George, M**, **Coheur, P-F**, **Hurtmans, D**, **Bowman, KW**, **Luo, M**, **Payne, VH**, **Kulawik, SS**. 2021. Air pollution trends measured from Terra: CO and AOD over industrial, fire-prone, and background regions. *Remote Sensing of Environment* **256**: 112275. DOI: http://dx.doi.org/10.1016/j.rse.2020.112275.

Clark, H, **Bennouna, Y**, **Tsivlidou, M**, **Wolff, P**, **Sauvage, B**, **Barret, B**, **Flochmoën, EL**, **Blot, R**, **Boulanger, D**, **Cousin, J-M**, **Nédélec, P**, **Petzold, A**, **Thouret, V**. 2021. The effects of the COVID-19 lockdowns on the composition of the troposphere as seen by In-service Aircraft for a Global Observing System (IAGOS) at Frankfurt. *Atmospheric Chemistry and Physics* **21**(21): 16237–16256. DOI: http://dx.doi.org/10.5194/acp-21-16237-2021.

Computational and Information Systems Laboratory. 2019. Cheyenne: SGI ICE XA Cluster. DOI: http://dx.doi.org/10.5065/D6RX99HX.

Cristofanelli, P, **Arduni, J**, **Serva, F**, **Calzolari, F**, **Bonasoni, P**, **Maurizio, B**, **Michela, M**, **Michael, S**, **Pamela, T**, **Davide, P**. 2021. Negative ozone anomalies at a high mountain site in northern Italy during 2020: A possible role of COVID-19 lockdowns? *Environmental Research Letters* **16**(7): 074029. DOI: http://dx.doi.org/10.1088/1748-9326/ac0b6a.

Danabasoglu, G, **Lamarque, JF**, **Bacmeister, J**, **Bailey, DA**, **DuVivier, AK**, **Edwards, J**, **Emmons, LK**, **Fasullo, J**, **Garcia, R**, **Gettelman, A**, **Hannay, C**, **Holland, MM**, **Large, WG**, **Lauritzen, PH**, **Lawrence, DM**, **Lenaerts, JTM**, **Lindsay, K**, **Lipscomb, WH**, **Mills, MJ**, **Neale, R**, **Oleson, KW**, **Otto-Bliesner, B**, **Phillips, AS**, **Sacks, W**, **Tilmes, S**, **van Kampenhout, L**, **Vertenstein, M**, **Bertini, A**, **Dennis, J**, **Deser, C**, **Fischer, C**, **Fox-Kemper, B**, **Kay, JE**, **Kinnison, D**, **Kushner, PJ**, **Larson, VE**, **Long, MC**, **Mickelson, S**, **Moore, JK**, **Nienhouse, E**, **Polvani, L**, **Rasch, PJ**, **Strand, WG**. 2020. The community earth system model version 2 (CESM2). *Journal of Advances in Modeling Earth Systems* **12**(2): e2019MS001916. DOI: http://dx.doi.org/10.1029/2019MS001916.

Darmenov, A, **da Silva, AM.** 2014. The QuickFire emissions dataset (QFED)–Documentation of versions 2. 1, 2.2 and 2.4. *NASATM-2013-104606* **35**: 183.

Deroubaix, A, **Brasseur, G**, **Gaubert, B**, **Labuhn, I**, **Menut, L**, **Siour, G**, **Tuccella, P**. 2021. Response of surface ozone concentration to emission reduction and meteorology during the COVID-19 lockdown in Europe. *Meteorological Applications* **28**(3): e1990. DOI: http://dx.doi.org/10.1002/met.1990.

Doumbia, T, **Granier, C**, **Elguindi, N**, **Bouarar, I**, **Darras, S**, **Brasseur, G**, **Gaubert, B**, **Liu, Y**, **Shi, X**, **Stavrakou, T**, **Tilmes, S**, **Lacey, F**, **Deroubaix, A**, **Wang, T**. 2021. Changes in global air pollutant emissions during the COVID-19 pandemic: A dataset for atmospheric modeling. *Earth System Science Data* **13**(8): 4191–4206. DOI: http://dx.doi.org/10.5194/essd-13-4191-2021.

Drummond, JR, **Zou, J**, **Nichitiu, F**, **Kar, J**, **Deschambaut, R**, **Hackett, J**. 2010. A review of 9-year performance and operation of the MOPITT instrument. *Advances in Space Research* **45**(6): 760–774. DOI: http://dx.doi.org/10.1016/j.asr.2009.11.019.

Emmons, LK, **Hess, PG**, **Lamarque, JF**, **Pfister, GG.** 2012. Tagged ozone mechanism for MOZART-4, CAM-chem and other chemical transport models. *Geoscientific Model Development* **5**(6): 1531–1542. DOI: http://dx.doi.org/10.5194/gmd-5-1531-2012.

Emmons, LK, **Schwantes, RH**, **Orlando, JJ**, **Tyndall, G**, **Kinnison, D**, **Lamarque, J-F**, **Marsh, D**, **Mills, MJ**, **Tilmes, S**, **Bardeen, C**, **Buchholz, RR**, **Conley, A**, **Gettelman, A**, **Garcia, R**, **Simpson, I**, **Blake, DR**, **Meinardi, S**, **Pétron, G**. 2020. The Chemistry Mechanism in the Community Earth System Model Version 2 (CESM2). *Journal of Advances in Modeling Earth Systems* **12**(4): e2019MS001882. DOI: http://dx.doi.org/10.1029/2019MS001882.

Franco, B, **Bader, W**, **Toon, G**, **Bray, C**, **Perrin, A**, **Fischer, EV**, **Sudo, K**, **Boone, CD**, **Bovy, B**, **Lejeune, B**, **Servais, C**, **Mahieu, E**. 2015. Retrieval of ethane from ground-based FTIR solar spectra using improved spectroscopy: Recent burden increase above Jungfraujoch. *Journal of Quantitative Spectroscopy and Radiative Transfer* **160**: 36–49. DOI: http://dx.doi.org/10.1016/j.jqsrt.2015.03.017.

Gaubert, B, **Bouarar, I**, **Doumbia, T**, **Liu, Y**, **Stavrakou, T**, **Deroubaix, A**, **Darras, S**, **Elguindi, N**, **Granier, C**, **Lacey, F**, **Müller, J-F**, **Shi, X**, **Tilmes, S**, **Wang, T**, **Brasseur, GP**. 2021. Global changes in secondary atmospheric pollutants during the 2020 COVID-19 pandemic. *Journal of Geophysical Research: Atmospheres* **126**(8): e2020JD034213. DOI: http://dx.doi.org/10.1029/2020JD034213.

Gaubert, B, **Darras, S**, **Doumbia, T**, **Granier, C**, **Soulié, A**, **Tilmes, S**. 2023. 2020 CAM-chem Simulations.

Version 1.0. UCAR/NCAR - GDEX. DOI: https://doi.org/10.5065/c3cb-dv78. Accessed May 12, 2023.

Gaubert, B, **Emmons, LK**, **Raeder, K**, **Tilmes, S**, **Miyazaki, K**, **Arellano, AF Jr**, **Elguindi, N**, **Granier, C**, **Tang, W**, **Barré, J**, **Worden, HM**, **Buchholz, RR**, **Edwards, DP**, **Franke, P**, **Anderson, JL**, **Saunois, M**, **Schroeder, J**, **Woo, J-H**, **Simpson, IJ**, **Blake, DR**, **Meinardi, S**, **Wennberg, PO**, **Crounse, J**, **Teng, A**, **Kim, M**, **Dickerson, RR**, **He, H**, **Ren, X**, **Pusede, SE**, **Diskin, GS.** 2020. Correcting model biases of CO in East Asia: Impact on oxidant distributions during KORUS-AQ. *Atmospheric Chemistry and Physics* **20**(23): 14617–14647. DOI: http://dx.doi.org/10.5194/acp-20-14617-2020. Available at https://acp.copernicus.org/articles/20/14617/2020/.

Gaubert, B, **Worden, HM**, **Arellano, AFJ**, **Emmons, LK**, **Tilmes, S**, **Barré, J**, **Martinez Alonso, S**, **Vitt, F**, **Anderson, JL**, **Alkemade, F**, **Houweling, S**, **Edwards, DP**. 2017. Chemical feedback from decreasing carbon monoxide emissions. *Geophysical Research Letters* **44**(19): 9985–9995. DOI: http://dx.doi.org/10.1002/2017GL074987.

Gelaro, R, **McCarty, W**, **Suárez, MJ**, **Todling, R**, **Molod, A**, **Takacs, L**, **Randles, CA**, **Darmenov, A**, **Bosilovich, MG**, **Reichle, R**, **Wargan, K**, **Coy, L**, **Cullather, R**, **Draper, C**, **Akella, S**, **Buchard, V**, **Conaty, A**, **da Silva, AM**, **Gu, W**, **Kim, G-K**, **Koster, R**, **Lucchesi, R**, **Merkova, D**, **Nielsen, JE**, **Partyka, G**, **Pawson, S**, **Putman, W**, **Rienecker, M**, **Schubert, SD**, **Sienkiewicz, M**, **Zhao, B**. 2017. The Modern-Era Retrospective Analysis for Research and Applications, Version 2 (MERRA-2). *Journal of Climate* **30**(14): 5419–5454. DOI: http://dx.doi.org/10.1175/JCLI-D-16-0758.1.

Gkatzelis, GI, **Gilman, JB**, **Brown, SS**, **Eskes, H**, **Gomes, AR**, **Lange, AC**, **McDonald, BC**, **Peischl, J**, **Petzold, A**, **Thompson, CR**, **Kiendler-Scharr, A**. 2021. The global impacts of COVID-19 lockdowns on urban air pollution: A critical review and recommendations. *Elementa: Science of the Anthropocene* **9**(1): 00176. DOI: http://dx.doi.org/10.1525/elementa.2021.00176.

Grange, SK, **Lee, JD**, **Drysdale, WS**, **Lewis, AC**, **Hueglin, C**, **Emmenegger, L**, **Carslaw, DC**. 2021. COVID-19 lockdowns highlight a risk of increasing ozone pollution in European urban areas. *Atmospheric Chemistry and Physics* **21**(5): 4169–4185. DOI: http://dx.doi.org/10.5194/acp-21-4169-2021. Available at https://acp.copernicus.org/articles/21/4169/2021/.

Guenther, AB, **Jiang, X**, **Heald, CL**, **Sakulyanontvittaya, T**, **Duhl, T**, **Emmons, LK**, **Wang, X**. 2012. The Model of Emissions of Gases and Aerosols from Nature version 2.1 (MEGAN2.1): An extended and updated framework for modeling biogenic emissions. *Geoscientific Model Development* **5**(6): 1471–1492. DOI: http://dx.doi.org/10.5194/gmd-5-1471-2012. Available at https://www.geosci-model-dev.net/5/1471/2012/.

Hannigan, JW, **Ortega, I**, **Shams, SB**, **Blumenstock, T**, **Campbell, JE**, **Conway, S**, **Flood, V**, **Garcia, O**, **Griffith, D**, **Grutter, M**, **Hase, F**, **Jeseck, P**, **Jones, N**, **Mahieu, M**, **Makarova, M**, **De Mazière, M**, **Morino, I**, **Murata, I**, **Nagahama, T**, **Nakijima, H**, **Notholt, J**, **Palm, M**, **Poberovskii, A**, **Rettinger, M**, **Robinson, J**, **Röhling, AN**, **Schneider, M**, **Servais, C**, **Smale, D**, **Stremme, W**, **Strong, K**, **Sussmann, R**, **Te, Y**, **Vigouroux, C**, **Wizenberg, T**. 2022. Global atmospheric OCS trend analysis from 22 NDACC stations. *Journal of Geophysical Research: Atmospheres* **127**(4): e2021JD035764. DOI: http://dx.doi.org/10.1029/2021JD035764.

Hase, F, **Hannigan, JW**, **Coffey, MT**, **Goldman, A**, **Höpfner, M**, **Jones, NB**, **Rinsland, CP**, **Wood, SW**. 2004. Intercomparison of retrieval codes used for the analysis of high-resolution, ground-based FTIR measurements. *Journal of Quantitative Spectroscopy and Radiative Transfer* **87**(1): 25–52. DOI: http://dx.doi.org/10.1016/j.jqsrt.2003.12.008.

Herzen, J, **Lässig, F**, **Piazzetta, SG**, **Neuer, T**, **Tafti, L**, **Raille, G**, **Van Pottelbergh, T**, **Pasieka, M**, **Skrodzki, A**, **Huguenin, N**, **Dumonal, M**, **Kościsz, J**, **Bader, D**, **Gusset, F**, **Benheddi, M**, **Williamson, C**, **Kosinski, M**, **Petrik, M**, **Grosch, G**. 2022. Darts: User-friendly modern machine learning for time series. *The Journal of Machine Learning Research* **23**(1): 124:5442–124:5447.

Holt, CC. 2004. Forecasting seasonals and trends by exponentially weighted moving averages. *International Journal of Forecasting* **20**(1): 5–10. DOI: http://dx.doi.org/10.1016/j.ijforecast.2003.09.015.

Kalnay, E, **Kanamitsu, M**, **Kistler, R**, **Collins, W**, **Deaven, D**, **Gandin, L**, **Iredell, M**, **Saha, S**, **White, G**, **Woollen, J**, **Zhu, Y**, **Chelliah, M**, **Ebisuzaki, W**, **Higgins, W**, **Janowiak, J**, **Mo, KC**, **Ropelewski, C**, **Wang, J**, **Leetmaa, A**, **Reynolds, R**, **Jenne, R**, **Joseph, D**. 1996. The NCEP/NCAR 40-year reanalysis project. *Bulletin of the American Meteorological Society* **77**(3): 437–472. DOI: http://dx.doi.org/10.1175/1520-0477(1996)077<0437:TNYRP>2.0.CO;2.

Kroll, JH, **Heald, CL**, **Cappa, CD**, **Farmer, DK**, **Fry, JL**, **Murphy, JG**, **Steiner, AL**. 2020. The complex chemical effects of COVID-19 shutdowns on air quality. *Nature Chemistry* **12**(9): 777–779. DOI: http://dx.doi.org/10.1038/s41557-020-0535-z.

Laughner, JL, **Neu, JL**, **Schimel, D**, **Wennberg, PO**, **Barsanti, K**, **Bowman, KW**, **Chatterjee, A**, **Croes, BE**, **Fitzmaurice, HL**, **Henze, DK**, **Kim, J**, **Kort, EA**, **Liu, Z**, **Miyazaki, K**, **Turner, AJ**, **Anenberg, S**, **Avise, J**, **Cao, H**, **Crisp, D**, **de Gouw, J**, **Eldering, A**, **Fyfe, JC**, **Goldberg, DL**, **Gurney, KR**, **Hasheminassab, S**, **Hopkins, F**, **Ivey, CE**, **Jones, DBA**, **Liu, J**, **Lovenduski, NS**, **Martin, RV**, **McKinley, GA**, **Ott, L**, **Poulter, B**, **Ru, M**, **Sander, SP**, **Swart, N**, **Yung, YL**, **Zeng, Z-C**. 2021. Societal shifts due to COVID-19 reveal large-scale complexities and feedbacks between atmospheric chemistry and climate change. *Proceedings of the National Academy of*

Sciences **118**(46): e2109481118. DOI: http://dx.doi.org/10.1073/pnas.2109481118.

Levelt, PF, **Stein Zweers, DC**, **Aben, I**, **Bauwens, M**, **Borsdorff, T**, **De Smedt, I**, **Eskes, HJ**, **Lerot, C**, **Loyola, DG**, **Romahn, F**, **Stavrakou, T**, **Theys, N**, **Van Roozendael, M**, **Veefkind, JP**, **Verhoelst, T**. 2021. Air quality impacts of COVID-19 lockdown measures detected from space using high spatial resolution observations of multiple trace gases from Sentinel-5P/TROPOMI. *Atmospheric Chemistry and Physics Discussions* **2021**: 1–53. DOI: http://dx.doi.org/10.5194/acp-2021-534.

Liu, X, **Ma, PL**, **Wang, H**, **Tilmes, S**, **Singh, B**, **Easter, RC**, **Ghan, SJ**, **Rasch, PJ**. 2016. Description and evaluation of a new four-mode version of the Modal Aerosol Module (MAM4) within version 5.3 of the Community Atmosphere Model. *Geoscientific Model Development* **9**(2): 505–522. DOI: http://dx.doi.org/10.5194/gmd-9-505-2016. Available at https://gmd.copernicus.org/articles/9/505/2016/.

Liu, Y, **Wang, T**, **Stavrakou, T**, **Elguindi, N**, **Doumbia, T**, **Granier, C**, **Bouarar, I**, **Gaubert, B**, **Brasseur, GP**. 2021. Diverse response of surface ozone to COVID-19 lockdown in China. *Science of The Total Environment* **789**: 147739. DOI: http://dx.doi.org/10.1016/j.scitotenv.2021.147739.

Manney, GL, **Livesey, NJ**, **Santee, ML**, **Froidevaux, L**, **Lambert, A**, **Lawrence, ZD**, **Millán, LF**, **Neu, JL**, **Read, WG**, **Schwartz, MJ**, **Fuller, RA**. 2020. Record-low arctic stratospheric ozone in 2020: MLS observations of chemical processes and comparisons with previous extreme winters. *Geophysical Research Letters* **47**(16): e2020GL089063. DOI: http://dx.doi.org/10.1029/2020GL089063. Available at https://onlinelibrary.wiley.com/doi/pdf/10.1029/2020GL089063.

McNorton, J, **Bousserez, N**, **Agust-Panareda, A**, **Balsamo, G**, **Cantarello, L**, **Engelen, R**, **Huijnen, V**, **Inness, A**, **Kipling, Z**, **Parrington, M**, **Ribas, R**. 2022. Quantification of methane emissions from hotspots and during COVID-19 using a global atmospheric inversion. *Atmospheric Chemistry and Physics* **22**(9): 5961–5981. DOI: http://dx.doi.org/10.5194/acp-22-5961-2022.

Mills, MJ, **Schmidt, A**, **Easter, R**, **Solomon, S**, **Kinnison, DE**, **Ghan, SJ**, **Neely III, RR**, **Marsh, DR**, **Conley, A**, **Bardeen, CG**, **Gettelman, A**. 2016. Global volcanic aerosol properties derived from emissions, 1990-2014, using CESM1(WACCM). *Journal of Geophysical Research: Atmospheres* **121**(5): 2332–2348. DOI: http://dx.doi.org/10.1002/2015JD024290.

Miyazaki, K, **Bowman, K**, **Sekiya, T**, **Takigawa, M**, **Neu, JL**, **Sudo, K**, **Osterman, G**, **Eskes, H**. 2021. Global tropospheric ozone responses to reduced NO_x emissions linked to the COVID-19 worldwide lockdowns. *Science Advances* **7**(24): eabf7460. DOI: http://dx.doi.org/10.1126/sciadv.abf7460.

Nussbaumer, CM, **Pozzer, A**, **Tadic, I**, **Röder, L**, **Obersteiner, F**, **Harder, H**, **Lelieveld, J**, **Fischer, H**. 2022. Tropospheric ozone production and chemical regime analysis during the COVID-19 lockdown over Europe. *Atmospheric Chemistry and Physics* **22**(9): 6151–6165. DOI: http://dx.doi.org/10.5194/acp-22-6151-2022. Available at https://acp.copernicus.org/articles/22/6151/2022/.

Ordóñez, C, **Garrido-Perez, JM**, **Garca-Herrera, R.** 2020. Early spring near-surface ozone in Europe during the COVID-19 shutdown: Meteorological effects outweigh emission changes. *Science of The Total Environment* **747**: 141322. DOI: http://dx.doi.org/10.1016/j.scitotenv.2020.141322.

Ortega, I, **Hannigan, J**, **Buchholz, R**, **Pfister, G.** 2021. Long-term variability and source signature of gases emitted from oil & natural gas and cattle feedlot operations in the Colorado front range. *Atmospheric Environment* **263**: 118663. DOI: http://dx.doi.org/10.1016/j.atmosenv.2021.118663.

Peng, S, **Lin, X**, **Thompson, RL**, **Xi, Y**, **Liu, G**, **Hauglustaine, D**, **Lan, X**, **Poulter, B**, **Ramonet, M**, **Saunois, M**, **Yin, Y**, **Zhang, Z**, **Zheng, B**, **Ciais, P**. 2022. Wetland emission and atmospheric sink changes explain methane growth in 2020. *Nature* **612**(7940): 477–482. DOI: http://dx.doi.org/10.1038/s41586-022-05447-w.

Qu, Z, **Jacob, DJ**, **Zhang, Y**, **Shen, L**, **Varon, DJ**, **Lu, X**, **Scarpelli, T**, **Bloom, A**, **Worden, J**, **Parker, RJ**. 2022. Attribution of the 2020 surge in atmospheric methane by inverse analysis of GOSAT observations. *Environmental Research Letters* **17**(9): 094003. DOI: http://dx.doi.org/10.1088/1748-9326/ac8754.

Reifenberg, SF, **Martin, A**, **Kohl, M**, **Bacer, S**, **Hamryszczak, Z**, **Tadic, I**, **Röder, L**, **Crowley, DJ**, **Fischer, H**, **Kaiser, K**, **Schneider, J**, **Dörich, R**, **Crowley, JN**, **Tomsche, L**, **Marsing, A**, **Voigt, C**, **Zahn, A**, **Pöhlker, C**, **Holanda, BA**, **Krüger, O**, **Pöschl, U**, **Pöhlker, M**, **Jöckel, P**, **Dorf, M**, **Schumann, U**, **Williams, J**, **Bohn, B**, **Curtius, J**, **Harder, H**, **Schlager, H**, **Lelieveld, J**, **Pozzer, A**. 2022. Numerical simulation of the impact of COVID-19 lockdown on tropospheric composition and aerosol radiative forcing in Europe. *Atmospheric Chemistry and Physics* **22**(16): 10901–10917. DOI: http://dx.doi.org/10.5194/acp-22-10901-2022. Available at https://acp.copernicus.org/articles/22/10901/2022/.

Rodgers, CD. 2000. *Inverse methods for atmospheric sounding: Theory and practice*. Singapore, Singapore: World Scientific.

Rodgers, CD, **Connor, BJ.** 2003. Intercomparison of remote sounding instruments. *Journal of Geophysical Research: Atmospheres* **108**: 4116. DOI: http://dx.doi.org/10.1029/2002JD002299.

Salawitch, RJ, **McBride, LA.** 2022. Australian wildfires depleted the ozone layer. *Science* **378**(6622): 829–830. DOI: http://dx.doi.org/10.1126/science.add2056.

Sha, MK, **Langerock, B**, **Blavier, JFL**, **Blumenstock, T**, **Borsdorff, T**, **Buschmann, M**, **Dehn, A**, **De Mazière, M**, **Deutscher, NM**, **Feist, DG**, **García, OE**, **Griffith, DWT**, **Grutter, M**, **Hannigan, JW**, **Hase, F**, **Heikkinen, P**, **Hermans, C**, **Iraci, LT**,

Jeseck, P, **Jones, N**, **Kivi, R**, **Kumps, N**, **Landgraf, J**, **Lorente, A**, **Mahieu, E**, **Makarova, MV**, **Mellqvist, J**, **Metzger, J-M**, **Morino, I**, **Nagahama, T**, **Notholt, J**, **Ohyama, H**, **Ortega, I**, **Palm, M**, **Petri, C**, **Pollard, DF**, **Rettinger, M**, **Robinson, J**, **Roche, S**, **Roehl, CM**, **Röhling, AN**, **Rousogenous, C**, **Schneider, M**, **Shiomi, K**, **Smale, D**, **Stremme, W**, **Strong, K**, **Sussmann, R**, **Té, Y**, **Uchino, O**, **Velazco, VA**, **Vigouroux, C**, **Vrekoussis, M**, **Wang, P**, **Warneke, T**, **Wizenberg, T**, **Wunch, D**, **Yamanouchi, S**, **Yang, Y**, **Zhou, M**. 2021. Validation of methane and carbon monoxide from Sentinel-5 Precursor using TCCON and NDACC-IRWG stations. *Atmospheric Measurement Techniques* **14**(9): 6249–6304. DOI: http://dx.doi.org/10.5194/amt-14-6249-2021.

Sokhi, RS, **Singh, V**, **Querol, X**, **Finardi, S**, **Targino, AC**, **de Fatima Andrade, M**, **Pavlovic, R**, **Garland, RM**, **Massagué, J**, **Kong, S**, **Baklanov, A**, **Ren, L**, **Tarasova, O**, **Carmichael, G**, **Peuch, V-H**, **Anand, V**, **Arbilla, G**, **Badali, K**, **Beig, G**, **Belalcazar, LC**, **Bolignano, A**, **Brimblecombe, P**, **Camacho, P**, **Casallas, A**, **Charland, J-P**, **Choi, J**, **Chourdakis, E**, **Coll, I**, **Collins, M**, **Cyrys, J**, **da Silva, CM**, **Giosa, ADD**, **Leo, AD**, **Ferro, C**, **Gavidia-Calderon, M**, **Gayen, A**, **Ginzburg, A**, **Godefroy, F**, **Gonzalez, YA**, **Guevara-Luna, M**, **Haque, SkM**, **Havenga, H**, **Herod, D**, **Hõrrak, U**, **Hussein, T**, **Ibarra, S**, **Jaimes, M**, **Kaasik, M**, **Khaiwal, R**, **Kim, J**, **Kousa, A**, **Kukkonen, J**, **Kulmala, M**, **Kuula, J**, **Violette, NL**, **Lanzani, G**, **Liu, X**, **MacDougall, S**, **Manseau, PM**, **Marchegiani, G**, **McDonald, B**, **Mishra, SV**, **Molina, LT**, **Mooibroek, D**, **Mor, S**, **Moussiopoulos, N**, **Murena, F**, **Niemi, JV**, **Noe, S**, **Nogueira, T**, **Norman, M**, **Pérez-Camaño, JL**, **Petäjä, T**, **Piketh, S**, **Rathod, A**, **Reid, K**, **Retama, A**, **Rivera, O**, **Rojas, NY**, **Rojas-Quincho, JP**, **José, RS**, **Sánchez, O**, **Seguel, RJ**, **Sillanpää, S**, **Su, Y**, **Tapper, N**, **Terrazas, A**, **Timonen, H**, **Toscano, D**, **Tsegas, G**, **Velders, GJM**, **Vlachokostas, C**, **von Schneidemesser, E**, **Rajasree, VPM**, **Yadav, R**, **Zalakeviciute, R**, **Zavala, M**. 2021. A global observational analysis to understand changes in air quality during exceptionally low anthropogenic emission conditions. *Environment International* **157**: 106818. DOI: http://dx.doi.org/10.1016/j.envint.2021.106818.

Soulie, A, **Granier, C**, **Darras, S**, **Doumbia, T**, **Guevara, M**, **Jalkanen, J-P**, **Keita, S**, **Liousse, C**, **Crippa, M**, **Guizzardi, D**, **Smith, S**. 2023. Global anthropogenic emissions (CAMS-GLOB-ANT) for the copernicus atmosphere monitoring service air quality forecasting and reanalyses. *Earth System Science Data*, submitted, under review.

Stavrakou, T, **Müller, JF**, **Bauwens, M**, **Doumbia, T**, **Elguindi, N**, **Darras, S**, **Granier, C**, **Smedt, ID**, **Lerot, C**, **Roozendael, MV**, **Franco, B**, **Clarisse, L**, **Clerbaux, C**, **Coheur, P-F**, **Liu, Y**, **Wang, T**, **Shi, X**, **Gaubert, B**, **Tilmes, S**, **Brasseur, G**. 2021. Atmospheric impacts of COVID-19 on NO_x and VOC levels over China based on TROPOMI and IASI Satellite Data and Modeling. *Atmosphere* **12**(8). DOI: http://dx.doi.org/10.3390/atmos12080946.

Steinbrecht, W, **Kubistin, D**, **Plass-Dülmer, C**, **Davies, J**, **Tarasick, DW**, **von der Gathen, P**, **Deckelmann, H**, **Jepsen, N**, **Kivi, R**, **Lyall, N**, **Palm, M**, **Notholt, J**, **Kois, B**, **Oelsner, P**, **Allaart, M**, **Piters, A**, **Gill, M**, **Malderen, RV**, **Delcloo, AW**, **Sussmann, R**, **Mahieu, E**, **Servais, C**, **Romanens, G**, **Stübi, R**, **Ancellet, G**, **Godin-Beekmann, S**, **Yamanouchi, S**, **Strong, K**, **Johnson, B**, **Cullis, P**, **Petropavlovskikh, I**, **Hannigan, JW**, **Hernandez, J-L**, **Rodriguez, AD**, **Nakano, T**, **Chouza, F**, **Leblanc, T**, **Torres, C**, **Garcia, O**, **Röhling, AN**, **Schneider, M**, **Blumenstock, T**, **Tully, M**, **Paton-Walsh, C**, **Jones, N**, **Querel, R**, **Strahan, S**, **Stauffer, RM**, **Thompson, AM**, **Inness, A**, **Engelen, R**, **Chang, K-L**, **Cooper, OR**. 2021. COVID-19 crisis reduces free tropospheric ozone across the northern hemisphere. *Geophysical Research Letters* **48**(5): e2020GL091987. DOI: http://dx.doi.org/10.1029/2020GL091987.

Stevenson, DS, **Derwent, RG**, **Wild, O**, **Collins, WJ.** 2022. COVID-19 lockdown emission reductions have the potential to explain over half of the coincident increase in global atmospheric methane. *Atmospheric Chemistry and Physics* **22**(21): 14243–14252. DOI: http://dx.doi.org/10.5194/acp-22-14243-2022.

Sun, W, **Zhu, L**, **De Smedt, I**, **Bai, B**, **Pu, D**, **Chen, Y**, **Shu, L**, **Wang, D**, **Fu, T-M**, **Wang, X**, **Yang, X**. 2021. Global significant changes in formaldehyde (HCHO) columns observed from space at the early stage of the COVID-19 pandemic. *Geophysical Research Letters* **48**(4): 2e020GL091265. DOI: http://dx.doi.org/10.1029/2020GL091265.

Viatte, C, **Strong, K**, **Walker, KA**, **Drummond, JR.** 2014. Five years of CO, HCN, C_2H_6, C_2H_2, CH_3OH, HCOOH and H_2CO total columns measured in the Canadian high Arctic. *Atmospheric Measurement Techniques* **7**(6): 1547–1570. DOI: http://dx.doi.org/10.5194/amt-7-1547-2014.

Vigouroux, C, **Bauer Aquino, CA**, **Bauwens, M**, **Becker, C**, **Blumenstock, T**, **De Mazière, M**, **García, O**, **Grutter, M**, **Guarin, C**, **Hannigan, J**, **Hase, F**, **Jones, N**, **Kivi, R**, **Koshelev, D**, **Langerock, B**, **Lutsch, E**, **Makarova, M**, **Metzger, J-M**, **Müller, J-F**, **Notholt, J**, **Ortega, I**, **Palm, M**, **Paton-Walsh, C**, **Poberovskii, A**, **Rettinger, M**, **Robinson, J**, **Smale, D**, **Stavrakou, T**, **Stremme, W**, **Strong, K**, **Sussmann, R**, **Té, Y**, **Toon, G**. 2018. NDACC harmonized formaldehyde time series from 21 FTIR stations covering a wide range of column abundances. *Atmospheric Measurement Techniques* **11**(9): 5049–5073. DOI: http://dx.doi.org/10.5194/amt-11-5049-2018.

Vigouroux, C, **Blumenstock, T**, **Coffey, M**, **Errera, Q**, **Garca, O**, **Jones, NB**, **Hannigan, JW**, **Hase, F**, **Liley, B**, **Mahieu, E**, **Mellqvist, J**, **Notholt, J**, **Palm, M**, **Persson, G**, **Schneider, M**, **Servais, C**, **Smale, D**, **Thölix, L**, **De Mazière, M**. 2015. Trends of ozone total columns and vertical distribution from FTIR observations at eight NDACC stations around the globe. *Atmospheric Chemistry and Physics* **15**(6):

2915–2933. DOI: http://dx.doi.org/10.5194/acp-15-2915-2015.

Vigouroux, C, **Stavrakou, T**, **Whaley, C**, **Dils, B**, **Duflot, V**, **Hermans, C**, **Kumps, N**, **Metzger, J-M**, **Scolas, F**, **Vanhaelewyn, G**, **Müller, J-F**, **Jones, DBA**, **Li, Q**, **De Mazière, M**. 2012. FTIR time-series of biomass burning products (HCN, C_2H_6, C_2H_2, CH_3OH, and HCOOH) at Reunion Island (21 S, 55 E) and comparisons with model data. *Atmospheric Chemistry and Physics* **12**(21): 10367–10385. DOI: http://dx.doi.org/10.5194/acp-12-10367-2012.

Worden, HM, **Deeter, MN**, **Frankenberg, C**, **George, M**, **Nichitiu, F**, **Worden, J**, **Aben, I**, **Bowman, KW**, **Clerbaux, C**, **Coheur, PF**, **de Laat, ATJ**, **Detweiler, R**, **Drummond, JR**, **Edwards, DP**, **Gille, JC**, **Hurtmans, D**, **Luo, M**, **Martínez-Alonso, S**, **Massie, S**, **Pfister, G**, **Warner, JX**. 2013. Decadal record of satellite carbon monoxide observations. *Atmospheric Chemistry and Physics* **13**(2): 837–850. DOI: http://dx.doi.org/10.5194/acp-13-837-2013.

Xiao, Y, **Jacob, DJ**, **Turquety, S.** 2007. Atmospheric acetylene and its relationship with CO as an indicator of air mass age. *Journal of Geophysical Research: Atmospheres* **112**(D12). DOI: http://dx.doi.org/10.1029/2006JD008268. Available at https://onlinelibrary.wiley.com/doi/abs/10.1029/2006JD008268.

Zhang, K, **Liu, Z**, **Zhang, X**, **Li, Q**, **Jensen, A**, **Tan, W**, **Huang, L**, **Wang, Y**, **de Gouw, J**, **Li, L**. 2022. Insights into the significant increase in ozone during COVID-19 in a typical urban city of China. *Atmospheric Chemistry and Physics* **22**(7): 4853–4866. DOI: http://dx.doi.org/10.5194/acp-22-4853-2022. Available at https://acp.copernicus.org/articles/22/4853/2022/.

Zhao, Y, **Saunois, M**, **Bousquet, P**, **Lin, X**, **Berchet, A**, **Hegglin, MI**, **Canadell, JG**, **Jackson, RB**, **Deushi, M**, **Jöckel, P**, **Kinnison, D**, **Kirner, O**, **Strode, S**, **Tilmes, S**, **Dlugokencky, EJ**, **Zheng, B**. 2020. On the role of trend and variability in the hydroxyl radical (OH) in the global methane budget. *Atmospheric Chemistry and Physics* **20**(21): 13011–13022. DOI: http://dx.doi.org/10.5194/acp-20-13011-2020.

Zhou, M, **Jiang, J**, **Langerock, B**, **Dils, B**, **Sha, MK**, **De Mazière, M**. 2021. Change of CO concentration due to the COVID-19 lockdown in China observed by surface and satellite observations. *Remote Sensing* **13**(6). DOI: http://dx.doi.org/10.3390/rs13061129.

Ziemke, JR, **Kramarova, NA**, **Frith, SM**, **Huang, LK**, **Haffner, DP**, **Wargan, K**, **Lamsal, LN**, **Labow, GJ**, **McPeters, RD**, **Bhartia, PK**. 2022. NASA satellite measurements show global-scale reductions in free tropospheric ozone in 2020 and again in 2021 during COVID-19. *Geophysical Research Letters* **49**(15): e2022GL098712. DOI: http://dx.doi.org/10.1029/2022GL098712. Available at https://agupubs.onlinelibrary.wiley.com/doi/abs/10.1029/2022GL098712.

How to cite this article: Ortega, I, Gaubert, B, Hannigan, JW, Brasseur, G, Worden, HM, Blumenstock, T, Fu, H, Hase, F, Jeseck, P, Jones, N, Liu, C, Mahieu, E, Morino, I, Murata, I, Notholt, J, Palm, M, Röhling, A, Té, Y, Strong, K, Sun, Y, Yamanouchi, S. 2023. Anomalies of O_3, CO, C_2H_2, H_2CO, and C_2H_6 detected with multiple ground-based Fourier-transform infrared spectrometers and assessed with model simulation in 2020: COVID-19 lockdowns versus natural variability. *Elementa: Science of the Anthropocene* 11(1). DOI: https://doi.org/10.1525/elementa.2023.00015

Domain Editor-in-Chief: Detlev Helmig, Boulder AIR LLC, Boulder, CO, USA

Associate Editor: Isobel Jane Simpson, Department of Chemistry, University of California, Irvine, Irvine, CA, USA

Knowledge Domain: Atmospheric Science

Published: May 22, 2023 **Accepted:** April 12, 2023 **Submitted:** January 05, 2023